scientific reports

Check for updates

OPEN

Performance enhancement of photovoltaic thermal collectors using water based MnO_2 nanofluids and machine learning models

M. P. Rajakumar[1], S. Senthil Kumar[2], B. Srimanickam[3], S. Srividhya[4], K. Elangovan[5], Nandagopal Kaliappan[6,7]✉ & K. Kamakshi Priya[8]

This study investigates the enhancement of Photovoltaic-Thermal (PVT) collector performance through the combined use of water-based manganese dioxide (MnO_2) nanofluids and machine learning (ML) models. Conventional PVT systems often suffer from elevated operating temperatures that degrade photovoltaic efficiency. To address this challenge, the research employs MnO_2 nanoparticles—known for their stability, cost-effectiveness, and high thermal conductivity—dispersed in water to improve thermal regulation within the PVT system. Experimental evaluations were conducted at three flow rates (0.5, 1.0, and 1.5 LPM) to assess thermal and electrical performance. The MnO_2 nanofluid-based PVT collector demonstrated superior power output (ranging from 80.42 W to 202.91 W) compared to water-cooled PVT (72.48 W to 176.17 W) and standalone PV systems (64.23 W to 152.36 W). A peak electrical efficiency of 14.58% was observed at 0.5 LPM, while glazing surface temperatures during midday ranged between 52.03 °C and 54.60 °C, indicating effective thermal management. To predict system behavior and performance, machine learning models—including Random Forest (RF), Radial Basis Function (RBF), and Multilayer Perceptron (MLP)—were applied. Among these, the RBF model achieved the highest predictive accuracy, with R^2 values of 0.96 for power output and 0.97 for electrical efficiency on the testing dataset. Overall, this integrated experimental-ML approach not only confirms the thermal and electrical advantages of MnO_2 nanofluids but also demonstrates the potential for intelligent optimization and control in high-performance solar energy systems.

Keywords Water, MnO_2, PVT, Power, Electrical efficiency, Machine learning, RF, RBF, MLP

Abbreviations

$\hat{E}_{el}$	Outlet electrical power (W)
$\hat{E}x_{el}$	Electrical Exergy (W)
$\hat{E}x_{th}$	Thermal Exergy (W)
$\hat{E}x_{out}$	Overall Exergy (W)
V_{mp}	Maximum power point voltage (volts)
I_{mp}	Maximum power point current (amps)
G	Solar radiation (W/m^2)
$\dot{S}$	Absorbed solar energy (W)
A_{mod}	PV module area (m^2)
L_1	Length of the PV module (m)
L_2	Breadth of the PV module (m)
Ns	Number of string

[1]Department of Artificial intelligence and Data Science, St.Joseph's College of Engineering, Chennai 600 119, India. [2]Department of Mechanical Engineering, R.M.K. College of Engineering and Technology, Puduvoyal 601206, Chennai, India. [3]Department of Mechanical Engineering, Cambridge Institute of Technology, Bengaluru 560036, Karnataka, India. [4]Department of ISE, BNM Institute of Technology, Bangalore, India. [5]Innovation Cell, Ministry of Education, New Delhi, India. [6]Department of Mechanical Engineering, Haramaya university, Harar, Ethiopia. [7]Department of Food Technology, Dhanalakshmi Srinivasan College of Engineering, Coimbatore, Tamil Nadu, India. [8]Department of Physics, Saveetha School of Engineering, SIMATS, Saveetha University, Chennai, Tamil Nadu, India. ✉email: raghugavaskarr@gmail.com

Nm	Number of module
$\dot{m}$	Mass flow rate of the coolant (kg/s)
C_p	Specific heat of air (kJ/kg K)
T_{in}	Input temperature of the collector (°C)
T_{out}	Output temperature of the collector (°C)
T_s	Surface temperature (°C)
T_a	Ambient temperature (°C)
A_{mod}	Area of the solar module (m^2)
$\dot{S}_{gen}$	Entropy generation (kJ/K)
η_{EX}	Exergy efficiency (%)
Q_0	Heat loss to the ambient (W)
Ex_{iire}	Irreversibility (kJ)
Q_s	Solar energy absorbed by panel surface (W)

The global quest for clean and renewable energy sources has highlighted the PVT systems, which can generate both electricity and heat energy from solar radiation. However, the efficiency of typical PVT systems is frequently limited by increased operating temperatures, which have a detrimental impact on photovoltaic electrical performance. Addressing this problem requires novel thermal management systems that can improve heat dissipation while maintaining electrical efficiency. In recent years, nanofluid fluids, which are created by scattering nanoparticles into base fluids, have emerged as viable options for enhancing their thermal conductivity and heat transmission in solar thermal systems. Manganese dioxide (MnO_2) nanoparticles stand out for their strong thermal conductivity, stability, and cost-effectiveness. MnO_2 particles suspended in water can improve thermal performance and energy efficiency in PVT systems.

Along with material improvements, the use of machine learning (ML) models provides a strong method for predicting and optimising the performance of complex systems such as PVT collectors. ML models can detect patterns and correlations among operational parameters using data-driven methodologies, allowing for accurate performance predictions and system optimisation in a variety of environments. This study intends to improve the performance of PVT collectors using water-based MnO_2 nanofluids and assess the system's behaviour using sophisticated machine learning algorithms. The work analyses the thermophysical advantages of MnO_2 nanofluids and shows how predictive analytics may enhance the design and real-time management of hybrid solar systems, resulting in more dependable and efficient renewable energy solutions.

The most pressing issue in today's global context is energy. Virtually every sector, including industrial, agricultural, medical, transportation, and residential, relies on energy, and this could lead to an over 30% increase in global energy consumption by 2035. Ensuring energy accessibility and availability is critical for both national and personal development. Given the impending depletion of fossil fuels like coal, natural gas, and oil, the development and utilization of renewable energy resources is crucial. Solar energy, in particular, stands out as one of the most effective renewable sources due to its cleanliness, abundance, and availability. Solar energy can be transformed into several usable forms, such as thermal, electrical, and chemical energy. Through the photovoltaic effect, solar cells convert incoming photons from the sun into electrical energy. However, as the temperature of the glazing surface increases, the energy output and efficiency of the solar panel decrease. To address this, various coolants such as air, water, and water-based nanofluids have been employed to enhance the panel's efficiency and increase energy output.

Solar energy and its photovoltaic heating system are among the most promising candidates for meeting the world's environmentally friendly energy needs. A critical aim is to ensure that solar photovoltaic (PV) cells work consistently over a wide range of operational circumstances[1]. Heat production in solar cells is a major source of efficiency loss in solar panels[2]. When solar cells convert sunlight to electricity, not all of the energy received is converted into electricity. A significant amount of the absorbed sunlight is transformed into heat by a variety of loss processes, including non-radiative charge carrier recombination and charge carrier thermalisation at higher energies. This heat production raises the cell's temperature, which degrades its performance by lowering the open-circuit voltage and conversion efficiency[3].

To increase photoelectric efficiency, a PVT (photovoltaic-thermal) collector is utilised, which generates both heat and electricity. Cooling the PV panel using an operating fluid within the PVT collector can increase photovoltaic efficiency. Furthermore, the integrated thermal collector in the PVT system improves heating efficiency, resulting in an overall rise in solar thermal efficiency[2,3]. Several recent strategies have been employed to enhance the performance of PVT systems. These methods involve using working fluids with improved thermal properties, either by adding nanoparticles or altering the absorber tube's cross-sectional shape to increase turbulence[4–6]. Sourav et al. conducted a thorough literature review on PV/T systems, emphasising the various electrical and thermal characteristics of photovoltaic-thermal systems. Their work includes studies on absorber design changes, development, and applications[7].

Various nanofluids, such as SiO_2, TiO_2, and $Al2O_3$ mixed with water[8], as well as CuO and SiC with water[9], have been used to improve the efficiency of the PVT collector and also carried out various parametric studies for its optimizations. However, limited research has focused on how different cross-sectional shapes of thermal collectors affect the operating temperatures and electrical efficiency of PVT systems[10,11]. Shakir et al.[12] conducted studies on a PVT system with three different water/nanofluids (ZnO, CuO, and TiO2) and a copper cooling channel. The electric effectiveness of the PVT with CuO/water was demonstrated to be 11.82%, whereas it was 11.61%, 11.52%, and 10.80% for water/ZnO, water/TiO2, and pure water, respectively.

A nanofluid/nano-PCM-based PVT system is presented in this work with the goal of increasing efficiency while lowering cost and space. A mathematical model that demonstrated a high degree of agreement with measurable data was constructed and confirmed experimentally. The system's thermal and electrical efficiency

were 72% and 13.7%, respectively. The highest observed temperatures were 41.2 °C for glass, 39.92 °C for PV cells, 38.8 °C for wax, and 36.5 °C for nanofluid. The verified model attests to its accuracy in representing the PVT system's hybrid cooling performance[13]. In order to lower PV cell temperatures and increase efficiency, this study assesses the thermal performance of a hybrid solar collector employing manganese oxide-water nanofluids as a coolant. To find the best performance, the system was tested at two flow rates (0.5 and 1.0 LPM). Maximum electrical and thermal efficiencies were 19.35% and 53.8% at 1.0 LPM, respectively.

The findings demonstrated that nanofluids had better thermal conductivity than base fluids. With only a little increase in flow rate, the hybrid collector showed enhanced energy efficiency and heat dissipation[6]. Attia et al.[14] used numerical analysis to assess the thermal performance of a PV/T system with air and water. The system was evaluated using two alternative flow configurations: a standard single straight zigzag plated flow and a three zigzag plated flow. Water and air-based systems outperformed standard PV/T systems in terms of thermal energy efficiency (ηth), increasing by 7.23% and 15.75%, respectively. Alkhalidi et al.[15] conducted an experimental investigation to evaluate the performance of open- and closed-loop PV/T systems at various tilt degrees. The study indicated that the open loop system had a greater overall energy efficiency (ηov) than the closed loop system, with a 31.04% advantage due to better thermal efficiency.

Amalraj et al. demonstrated that using nanofluids, particularly a combination of copper and aluminum nanofluids, effectively cooled solar panels[16]. Refaey et al.[17] experimented with Al2O3 nanoparticles at various volumetric concentrations and found that water-based nanofluids enhanced solar panel efficiency by mitigating heat loss, which is a key factor in efficiency reduction. It is important to note that not all of the energy received by solar cells is converted into electrical power[19]. Significant losses occur due to processes such as the thermalization of higher energy levels and the non-radiative recombination of charge carriers, resulting in heat generation. This heat raises the cell temperature and negatively impacts performance[20]. Prolonged exposure to high temperatures can also degrade the materials used in panels, further reducing efficiency. Therefore, managing heat dissipation and improving thermal management are essential for increasing solar panel efficiency and longevity[21].

Traditionally, theoretical equations derived from experiments and mathematical calculations have been used to predict a collector's efficiency. However, several irreversible drawbacks make this approach unreliable for researchers. For instance, many workbench parameters are either assumed or unknown and are not measured in catalog specifications[22]. Moreover, the nonlinear and polynomial electrical properties of PV cells require simultaneous solutions, which increases the risk of inaccurate results or even divergence during the problem-solving process. Additionally, the final outcome of simulations can become uncertain due to round-off errors accumulated from handling numerous equations and parameters. Fortunately, advancements in computer technology and the increased processing power of modern systems now enable researchers to overcome these limitations by employing machine learning (ML) techniques[23]. By harnessing the vast computational power available today, researchers can not only simplify the simulation of mathematical models but also significantly reduce processing costs and improve prediction accuracy[24].

Varol et al.[25] developed three predictive models—Artificial Neural Networks (ANN), Support Vector Machines (SVM), and Adaptive Neuro-Fuzzy Inference Systems (ANFIS)—to estimate the efficiency of collectors utilizing phase change materials (PCMs). Among these, the SVM model demonstrated superior accuracy. In another study, the influence of vortex generators (VGs) on a concentrating photovoltaic-thermal (CPVT) system with a parabolic solar concentrator and single-axis tracking in Najaf, Iraq, was experimentally assessed. The inclusion of VGs significantly improved cooling, resulting in a 15% increase in thermal efficiency and a 23% boost in electrical efficiency. Overall system efficiency rose from 64.31% (without VGs) to 74.81% (with VGs)[26]. Further advancements in CPVT performance were achieved through the integration of PCMs with porous foam and fins to enhance thermal storage. A parabolic reflector was used for solar concentration, and a directional optimization (DO) method analyzed heat flux distribution. A SiO_2-based self-cleaning coating reduced dust accumulation and improved liquid fraction (LF), while the PCM–foam–fins configuration improved electrical efficiency by 2.94%, reaching 13.35%[27].

Sheikholeslami and Khalili[28,29] explored the integration of thermoelectric generators (TEGs), PVT units, and electrolysers using novel wavy cooling duct designs and a ternary nanofluid (TiO_2–MgO–CuO in water). The impact of dust and hybrid nanofluid viscosity was assessed using machine learning (ML) models—Random Forest (RF), Gradient Boosting Regressor (GBR), Gaussian Regression (GR), and ANN—trained on 700 experimental data points. All models achieved $R^2 > 0.99$, with GBR emerging as the most accurate. Sankar et al.[30] introduced a hybrid ML framework combining Gaussian Process Regression (GPR) and a Genetic Algorithm (GA) for optimizing nanofluid-based solar collectors. This framework enabled multi-objective optimization and explainable sensitivity analysis, resulting in a 23.44 °C increase in outlet temperature, 37.48% rise in thermal efficiency, and 28.62% improvement in optical efficiency.

Alhamayani and Al-lehaibi[31] investigated the performance of parabolic trough solar collectors (PTSCs) using hybrid Al_2O_3–TiO_2 nanofluids with various thermal oils and molten salts. Among these, Therminol VP-1/Al_2O_3–TiO_2 achieved the highest thermal efficiency (71.68%), while Syltherm-800/Al_2O_3–TiO_2 exhibited the best exergy efficiency (24.1%). Solar Salt/Al_2O_3–TiO_2 also showed strong thermal (61.8%) and exergy (36.1%) performance. Kanti et al.[32] studied Al_2O_3–TiO_2 (50:50) nanofluids under turbulent flow. A 1% concentration enhanced the Nusselt number by 70.4% and reduced entropy generation by 46%. Viscosity increased moderately (15.77% at 30 °C). Predictive correlations and ML models confirmed the thermal benefits of hybrid nanofluids.

In hot climatic conditions like Riyadh, Alhamayani[33] employed various nanofluids and volume concentrations with deep learning to model PVT behavior. A CNN-LSTM model predicted PV temperatures with high accuracy (R^2 = 97.5–98.75%). CuO nanofluid (4% vol) reduced PV temperature by 34.5 °C and improved electrical (16.7%), thermal (79.2%), and exergy (18.07%) efficiencies. Similarly, in Tabuk, Saudi Arabia, a CNN-LSTM model trained on energy-balanced data achieved excellent prediction accuracy (R^2 = 98.3–99.3%) and reduced PV cell temperature to 43 °C, while improving thermal and electrical efficiencies by 15% and 9%, respectively[34].

Margoum et al.[35] evaluated three AI models—Extreme Gradient Boosting (XGB), Extra Trees Regressor (ETR), and K-Nearest Neighbors (KNN)—for estimating nanofluid-cooled PVT system performance. XGB yielded R^2 values up to 0.99999, outperforming others with minimal prediction error. Alhamayani[36] optimized Al_2O_3-MWCNT/Syltherm-800 hybrid nanofluid compositions using ML models (Decision Tree, SVM, ANN) for PTSCs. A 2% Al_2O_3 and 1% MWCNT blend achieved the highest thermal efficiency (70.54%). ANN emerged as the most accurate model (R^2 = 99.99%).

Sivamurugan et al.[11] studied the hybrid collector using a manganese oxide-water-based nanofluid as a coolant was investigated to improve the efficiency of solar photovoltaic (PV) units. The study found that using the nanofluid as a coolant significantly boosted both the electrical and thermal efficiencies of the system. Specifically, higher volume flow rates of the nanofluid led to better performance, with a flow rate of 1.0 LPM yielding the highest measured electrical and thermal efficiencies. This improvement is attributed to the nanofluid's superior thermal conductivity compared to the base fluid (water). Photovoltaic panel efficiency and lifespan are negatively impacted by high operating temperatures. This study investigated a photovoltaic/thermal (PVT) system using a multi-walled carbon nanotube/zinc oxide (MWCNT/ZnO) nanofluid as a coolant.

The research compared the performance of uncooled, water-cooled, and nanofluid-cooled panels, employing a low mass flow rate of 0.156 kg/min. The results showed that the nanofluid significantly enhanced the system's thermal properties, leading to notable improvements. Specifically, the MWCNT/ZnO nanofluid reduced the panel's maximum temperature by 14.9 °C, boosted average electrical efficiency by 16.8%, and achieved a maximum thermal efficiency of 51.3%. The system's overall efficiency with the nanofluid reached an impressive 58.7%, surpassing water-cooling. The nanofluid also improved exergy efficiency and reduced entropy generation compared to both conventional and water-cooled systems[37].

This review paper examines using nanofluids to improve the efficiency of photovoltaic (PV) systems by mitigating high operating temperatures. It explains the thermophysical properties of nanofluids that enable superior heat transfer compared to traditional coolants. The paper then analyzes how integrating nanofluids into photovoltaic-thermal (PVT) systems enhances both electrical and thermal output. The review highlights recent advances, documenting improvements in total energy and exergy efficiencies. It also addresses challenges such as nanofluid stability, cost, and environmental impact. The paper concludes by suggesting future research directions to optimize nanofluid technology for PV cooling, aiming to boost overall system efficiency[38]. Sharshir et al.[39] analysed the perovskite solar cells (PSCs) offer high efficiency and cost-effective production but face challenges with stability, toxicity, and scaling. This review paper focuses on the degradation of PSCs, driven by both external factors like temperature and humidity and internal factors such as ion migration and defects.

The research shows a strong correlation between increased defect density and reduced cell efficiency, which causing a significant drop in power conversion efficiency (PCE) from 21.69% to 8%. The study emphasizes that controlling environmental factors, particularly humidity, is critical for achieving optimal PSC performance, as evidenced by a higher PCE of 20.19% under controlled conditions versus 12.39% in high humidity. This research addresses the challenge of maximizing energy from photovoltaics (PVs) by combining a solar tracking system with a surface cooling technique. The study compared several PV configurations, including conventional fixed panels, fixed panels with spray cooling, and single-axis (SAT) and double-axis (DAT) tracking systems, both with cooling.

The findings show that while tracking systems significantly increase received solar radiation, the application of spray cooling effectively manages the resulting temperature rise. The greatest power generation increase was observed with the tracking systems, with the DAT system showing a notable 26.1% increase in power output and a peak efficiency of 14%[40]. Kandeal et al.[41] studied the solar tracking system with a surface cooling technique can maximize energy output from photovoltaics (PVs). The study compares the performance of fixed, single-axis tracking (SAT), and double-axis tracking (DAT) PV systems, with and without spray cooling. The findings demonstrate that tracking systems, particularly DAT, significantly increase solar energy capture and power generation. The use of spray cooling effectively manages the temperature increase caused by this higher solar exposure, resulting in the DAT system achieving a 26.1% increase in power output and a peak efficiency of 14%, confirming that this integrated approach is highly effective.

Sharshir et al.[42] investigated by experimentally using an Fe-Co-Al @ BTC Metal-Organic Framework (MOF) to enhance the evaporation rate in a double slope solar still (DSSS). The research tested three configurations: using the MOF as a nanofluid in the basin water (Case I), as a nanofluid with an atomizer (Case II), and for thin film evaporation (Case III). The results from a 4E analysis (Energy, Exergy, Economic, and Environmental) showed that all three configurations significantly improved the DSSS's performance compared to a conventional solar still (CSS). The thin film evaporation method (Case III) proved to be the most effective, showing the highest gains across all metrics. It increased energy efficiency by 103%, exergy efficiency by 162%, and accumulated distillate by 92.12%. Furthermore, Case III provided the best economic and environmental benefits, reducing freshwater cost by 26.22% and leading to substantial CO2 mitigation, which generated valuable carbon credits.

Despite numerous advances in PVT systems enhanced by nanofluids and AI, none of the reviewed works have experimentally assessed or modeled PVT systems using water-based manganese dioxide (MnO_2) nanofluids. This study addresses this gap by experimentally and computationally evaluating a water-based MnO_2 nanofluid-cooled PVT system, offering a significant advancement over conventional PV and water-cooled PVT configurations. MnO_2 nanoparticles, recognized for their thermal conductivity, stability, and cost-effectiveness, were used to improve cooling and lower PV surface temperatures, resulting in enhanced electrical efficiency. The system's performance was comprehensively analyzed across three flow rates (0.5, 1.0, and 1.5 LPM) and benchmarked against standalone PV and traditional water-based PVT collectors.

Furthermore, this study uniquely integrates machine learning models—Random Forest (RF), Radial Basis Function (RBF), and Multilayer Perceptron (MLP)—to forecast power output and electrical efficiency. The RBF model, in particular, effectively captured complex non-linear relationships, achieving superior predictive

accuracy (R^2 = 0.96–0.97), underscoring AI's capability in solar energy optimization. Overall, this integrated experimental-ML framework not only validates the thermal and electrical advantages of MnO_2 nanofluids but also establishes a robust foundation for intelligent design, real-time monitoring, and adaptive control of high-efficiency PVT systems, especially under varying flow and climatic conditions. The detailed summary of literature reviews were shown in Table 1.

A critical analysis of the extant literature reveals several persistent limitations that our study seeks to address. Firstly, while numerous nanofluids like silver (Ag) and carbon nanotubes (CNTs) have demonstrated exceptional thermal properties, their prohibitive cost and complex synthesis pathways severely hinder practical, large-scale deployment. Secondly, a significant body of work neglects the long-term stability of nanofluids, overlooking critical issues like nanoparticle aggregation, sedimentation, and corrosion, which degrade performance over time and are vital for real-world applications. Thirdly, many studies exhibit a narrow focus, prioritizing thermal performance enhancement often at the expense of a comprehensive energy-exergy analysis, thereby failing to capture the true thermodynamic quality of the energy output. Finally, the modeling approaches frequently rely on conventional theoretical or numerical methods, lacking integration with modern data-driven machine learning techniques for robust performance prediction and optimization. In direct response to these gaps, our work introduces a water-based MnO_2 nanofluid selected for its compelling balance of thermal conductivity, cost-effectiveness, and demonstrated stability and employs a holistic experimental-ML framework. This approach not only provides a complete energy and exergy assessment but also establishes accurate predictive models for system intelligence, offering a more viable and comprehensive solution for PVT system advancement.

Experimental description

Research site and testing procedure

The Chennai meteorological station is the location of the study site. Due to the great position that was chosen, there is intense sunlight here for about nine months. The duration of each parametric study was at least 6 to 7 days, which may be an average of the last day. The studies took place every day from 9 a.m. to 4 p.m. The sun will

Ref. no.	Nanofluid / coolant used	Experimental conditions	Type of PVT collector	Key outcomes
13	ZnO/water, CuO/water, TiO_2/water	Copper cooling channel	Flat Plate (assumed)	CuO/water yielded highest electrical effectiveness (11.82%). All nanofluids outperformed pure water (10.80%).
14	Nanofluid/Nano-PCM (type not specified)	Not specified	Hybrid Nano-PCM PVT	Achieved 72% thermal and 13.7% electrical efficiency. Validated a mathematical model with experimental data.
15	Manganese oxide (MnOx)/water	Flow rates: 0.5 & 1.0 LPM	Hybrid Solar Collector	Max efficiencies of 19.35% (electrical) and 53.8% (thermal) at 1.0 LPM.
16	Air and Water	Numerical study of zigzag flow configurations	Flat Plate with different flow channels	Zigzag flow improved thermal efficiency by 7.23% (water) and 15.75% (air).
17	Water (Open vs. Closed loop)	Various tilt angles	Open & Closed Loop PVT	Open-loop system had 31.04% better overall efficiency due to superior thermal performance.
18	Cu/Al hybrid nanofluid	Not specified	Flat Plate (assumed)	Demonstrated effective cooling of solar panels.
21	Al_2O_3/water	Various volumetric concentrations	Flat Plate (assumed)	Nanofluids enhanced efficiency by mitigating heat loss.
28	Not specified (Coolant likely water)	Parabolic concentrator, single-axis tracking	Concentrating PVT (CPVT)	Vortex generators (VGs) increased thermal efficiency by 15% and electrical by 23%.
29	Not specified (Coolant likely water)	Parabolic reflector, PCM with porous foam & fins	Concentrating PVT (CPVT)	PCM-foam-fins configuration improved electrical efficiency by 2.94% (to 13.35%).
30	Ternary nanofluid (TiO_2–MgO–CuO/water)	Novel wavy cooling ducts, ML analysis	Hybrid PVT-TEG-Electrolyser	All ML models achieved $R^2 > 0.99$ for predicting system performance.
32	Not specified (Nanofluid-based)	ML (GPR-GA) optimization	Solar Collector (General)	ML optimization led to a 37.48% rise in thermal efficiency and 28.62% improvement in optical efficiency.
33	Hybrid Al_2O_3–TiO_2 with oils/salts	Various thermal oils & molten salts	Parabolic Trough (PTSC)	Therminol VP-1/Al_2O_3–TiO_2 had best thermal efficiency (71.68%); Solar Salt mix had best exergy (36.1%).
34	Hybrid Al_2O_3–TiO_2 (50:50)	Turbulent flow, 1% concentration	Channel Flow (assumed)	Enhanced Nusselt number by 70.4%, reduced entropy generation by 46%.
35	CuO/water (4% vol)	Hot climate (Riyadh), DL modeling	Flat Plate PVT	Reduced PV temp by 34.5 °C; improved electrical (16.7%), thermal (79.2%), exergy (18.07%) efficiencies.
37	Not specified (Nanofluid)	Evaluation of AI models	Nanofluid-cooled PVT	XGB model achieved exceptional accuracy (R^2 up to 0.99999).
38	Hybrid Al_2O_3-MWCNT/Syltherm-800	ML optimization for PTSC	Parabolic Trough (PTSC)	2% Al_2O_3 & 1% MWCNT blend achieved 70.54% thermal efficiency. ANN was most accurate model (R^2=99.99%).
39	MWCNT/ZnO nanofluid	Low flow rate (0.156 kg/min)	Flat Plate PVT	Reduced panel temp by 14.9 °C, boosted electrical efficiency by 16.8%, max overall efficiency of 58.7%.
44	Fe-Co-Al @ BTC MOF (as nanofluid)	Double Slope Solar Still (DSSS)	Solar Still (Thermal)	Thin film evaporation increased energy efficiency by 103%, exergy by 162%, and distillate by 92.12%.
Present Study	Water-based MnO_2	Flow rates: 0.5, 1.0, 1.5 LPM	Flat Plate PVT	Superior performance over water & standalone PV. Achieved 14.58% electrical efficiency. RBF ML model best for prediction (R^2=0.96–0.97).

Table 1. Summary of literature reviews.

shine throughout this period, which will offer nature a lot of potential. In Chennai, India, the PVT collector was carried out in 2024 during the clear days of June and July. At 30-minute intervals during the steady state phase, the water and water-based MnO_2 volume rate, wind speed, and solar radiation were monitored and recorded in the Data Logger. The mercury thermometer is used to determine the day's average temperature. A digital surface temperature sensor was used to monitor the water passage temperatures at the inlet and outflow, the glazing surface temperature, and the tedlar temperature at 30-minute intervals.

Solar PV and solar PVT collector and its application

This research study included three different types of diagrams: solar PV, solar PVT, and its application. Another name for solar PV is an independent PV system. It was not equipped with any extra instrumentation. Sunlight hits the solar panel, causing it to reach its ambient temperature, glazing surface temperature, tedlar surface temperature, and solar radiation. Every temperature was noted at the data logger, which can be kept on the machine in consideration. Independent PV system is shown in Fig. 1.

The solar PVT collector consists of solar PV, centrifugal pump, small stainless steel cylinder, normal stainless steel cylinder, ammeter, voltmeter, regulator, valve, pipe fittings and related sub items. The water can be flowed from the water storage tank that passed by the regulator where 0.5, 1.0 and 1.5 L per minute were monitored and entered in the inlet of the solar PV. Then water moves which absorbs the heat from the tedlar side of the solar panel. Similarly, voltage and current were produced from the solar panel which can be stored in a storage device. This stored current will be used in street light as an application aspects. The street light was operated by the storage current during the essential hours of the day. Solar water and water based MnO_2 nano fluid PVT collector is presented in Fig. 2a. Various information of PVT collector configuration is found in Fig. 2b. Cross sectional view of PVT collector is shown in Fig. 2c. The generation of electricity is used in street light is found in Fig. 3. Description of PV and PVT collector is shown in Table 2.

MnO_2 nano particles and nano fluid experimental procedure

After adding 0.2 M of potassium permanganate to 100 mL of deionised water, the mixture was continuously stirred for approximately 40 min using a magnetic stirrer. When 0.1 M HCl (Hydrochloric acid) was gradually added while stirring constantly, the solution changed from purple to dark brown, signifying that the reaction had begun. After centrifuging, the precipitate was rinsed three times with deionised water and once with isopropanol. Ultimately, the powder was dried for 24 h at 100 °C in an oven. After that, a motor pistol was used to fine-grind it.

XRD studies

Figure 3 shows the XRD (X-ray Diffraction) structure of MnO_2. From this XRD pattern it was observed that the prepared nanoparticle is tetragonal structure. It also have well oriented (h k l) values like (1 0 1), (1 1 1), (2 2 0), (1 12) and (2 2 2) matches well with JCPDS No. 81-2261 (Joint Committee on Powder Diffraction Standards)[43].

Surface morphology and elemental analysis

Figure 4a Represents the SEM analysis of MnO_2 (Manganese dioxide) and (b) represents the EDAX spectrum of the MnO_2. It was observed from the SEM analysis; the prepared particle appears like stacks of grains which are properly arranged and also appears like tetragonal structure. The confirmation of Manganese and and Oxygen was confirmed from EDAX (Energy Dispersive X-ray Analysis or Energy Dispersive X-ray Spectroscopy) analysis. The presence of Cl (Chlorine) is due to HCL which was added to enhance the reaction.

X-ray Diffraction (XRD) is a potent, non-destructive analytical method that uses the diffraction patterns created when X-rays contact with a sample to ascertain the crystalline phase and structural characteristics of materials. The synthesised MnO_2 nanoparticles' tetragonal structure was accurately confirmed by XRD analysis (Fig. 3), which showed well-oriented (h k l) values that matched JCPDS No. 81-2261[43]. Its intended use depends on the effective synthesis of the desired material phase, which is rigorously validated by this. In contrast, Scanning Electron Microscopy (SEM) produces high-magnification pictures by using a concentrated electron beam to expose the particle's size, shape, arrangement, and surface morphology.

The visual evidence from our SEM examination (Fig. 4a) showed that the produced particles resemble "stacks of properly arranged grains," supporting the observed tetragonal structure and offering information on their physical properties related to heat transfer and dispersion stability. In addition to SEM, Energy Dispersive X-ray Analysis (EDAX) is an elemental analysis method that verifies the elemental composition of a sample by identifying distinctive X-rays released by it. Our synthesised MnO_2's chemical composition was validated by the presence of manganese (Mn) and oxygen (O), which were confirmed by EDAX analysis (Fig. 4b). In addition, a trace amount of chlorine (Cl) was found and linked to the HCl that was added throughout the synthesis process, indicating a comprehensive chemical characterisation.

By clearly describing the goals and conclusions of these characterisation methods and connecting them to our particular experimental outcomes, we want to offer enough context to promote comprehension and repeatability. This clear explanation of our materials synthesis and characterisation processes will enable other researchers to understand the characteristics of the MnO_2 nanoparticles we use, reproduce our techniques, and confidently build on our work, all of which will benefit the scientific community.

Durability & long-term stability

The evaluation of long-term stability, particularly concering nano particle which aggregation/sedimentation and corrosion, is a critical aspect for practical nanofluid application. Aggregation causes nanoparticles to clump and fall out of suspension, which degrades thermal conductivity and poses a risk of clogging flow channels, while their abrasive and chemically active nature can lead to the wear and corrosion of system components

Fig. 1. Independent PV system.

like pipes, pumps, and heat exchangers. The ideal response to this would involve conducting a full 1000-hour durability test; however, such an undertaking—representing over 41 days of continuous operation—was beyond the practical scope and timeline of this initial study, which instead focuses on establishing a foundational proof-of-concept for performance enhancement. A comprehensive investigation into long-term durability is a complex endeavor that is often appropriately reserved for a dedicated follow-up study.

We also conducted the following steps such as (1) Visual and Sedimentation Observation: The prepared nanofluid was observed for any visible sedimentation over a period of two weeks without any stirring. No

(a)

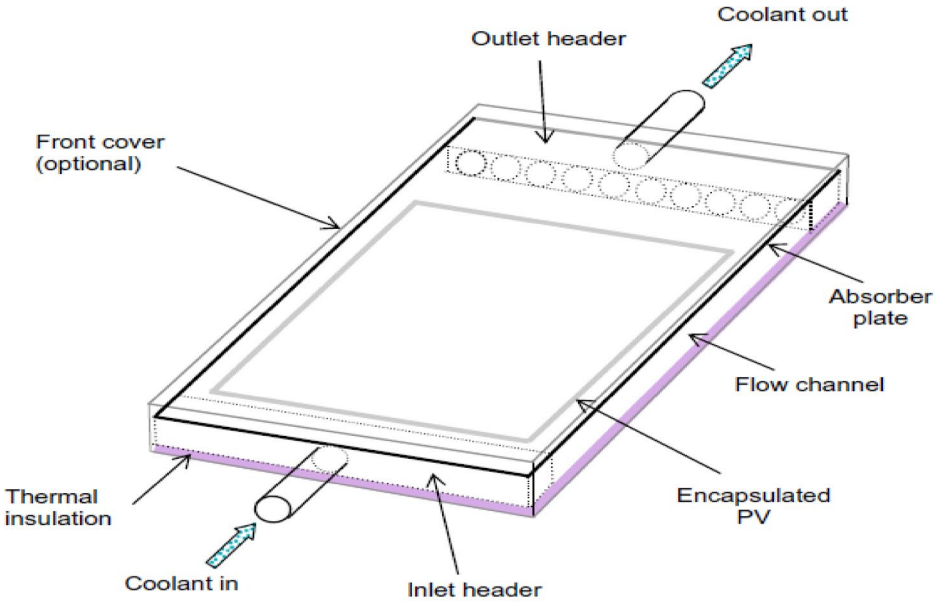

(b)

Fig. 2. (**a**) Solar water and water based MnO_2 nano fluid PVT collector. **(b)** Various information of PVT collector configuration. (**c**) Cross sectional view of PVT collector.

significant settling was observed, indicating good short-term colloidal stability (2) pH Monitoring: We monitored the pH of the nanofluid before and after the experimental trials. The minimal change in pH value suggests preliminary chemical stability. (3) Post-Experiment Inspection: A preliminary inspection of the flow loop components (pipes, pump) was conducted after the completion of all experimental tests. No signs of immediate corrosion or abrasion were noted.

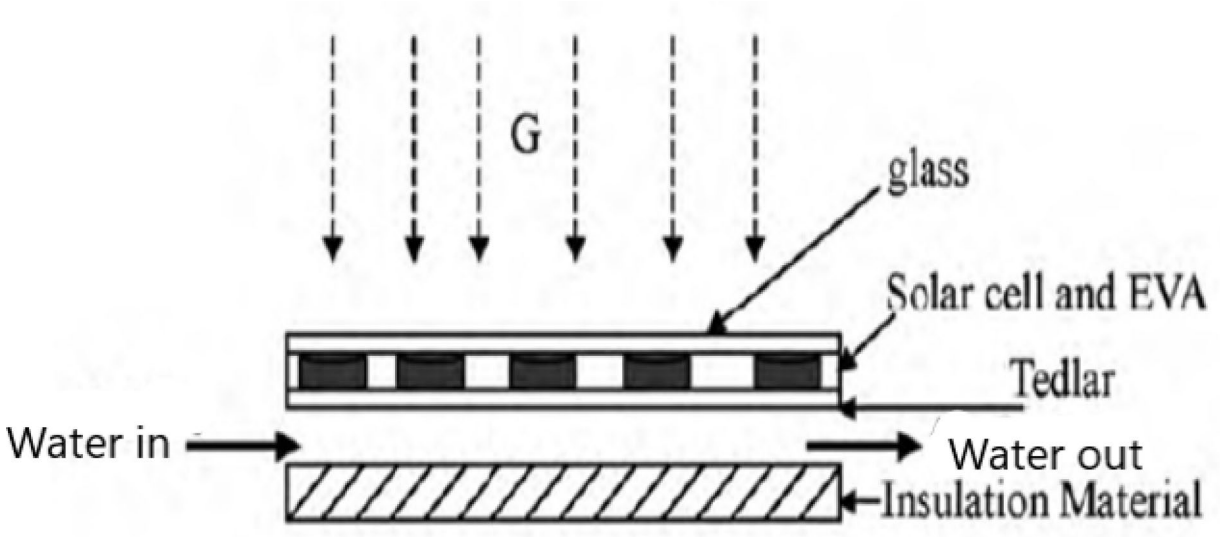

(c)

Fig. 2. (continued)

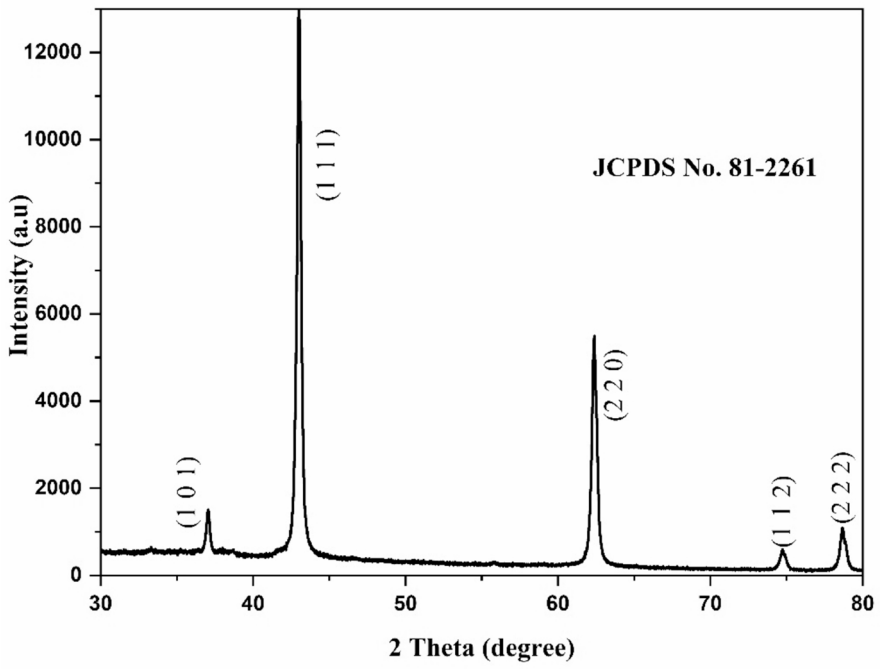

Fig. 3. XRD analysis of MnO_2.

Analytical methodology

Electrical efficiency calculation

The ratio of the actual electrical output power to the input rate of solar energy incident on the PV surface is known as the electrical efficiency of a PV module and maximum power point voltage (V_{mp}), maximum power point current (I_{mp}) and Electrical Exergy of the concern system ($\dot{E}x_{el}$) as follows[3,8,11].

$$\dot{E}x_{el}=\dot{E}_{\mathrm{el}} \tag{1}$$

$$\dot{E}_{\mathrm{el}} = \mathrm{V}_{\mathrm{mp}}\,\mathrm{I}_{\mathrm{mp}} \tag{2}$$

Portrayal	Values
Flow rate of water	0.5–1.5 LPM
Flow rate of MnO_2	0.5–1.5 LPM
Concentration of MnO_2	0.1 VL
Ambient temperature (Ta)	28–34 °C
Centrifugal pump	0.25 hp
Length of solar PV	1640 mm
Width of solar PV	992 mm
Thickness of solar PV	35 mm
Maximum system voltage	1000 V
Maximum series fuse rating	20 A
Current at P max	8.42 A
Voltage at P max	30.9 V
Short circuit current	8.89 A
Open circuit voltage	37.7 V
Inclination of solar panel	13°
Solar radiation (G)	425–1118 W/m^2
Gross weight of the solar panel	18.2 Kg
Model No.	AE689VBN1254
Brand	Panasonic
Cell Technology	Multi-silicon

Table 2. Description of PV and PVT collector.

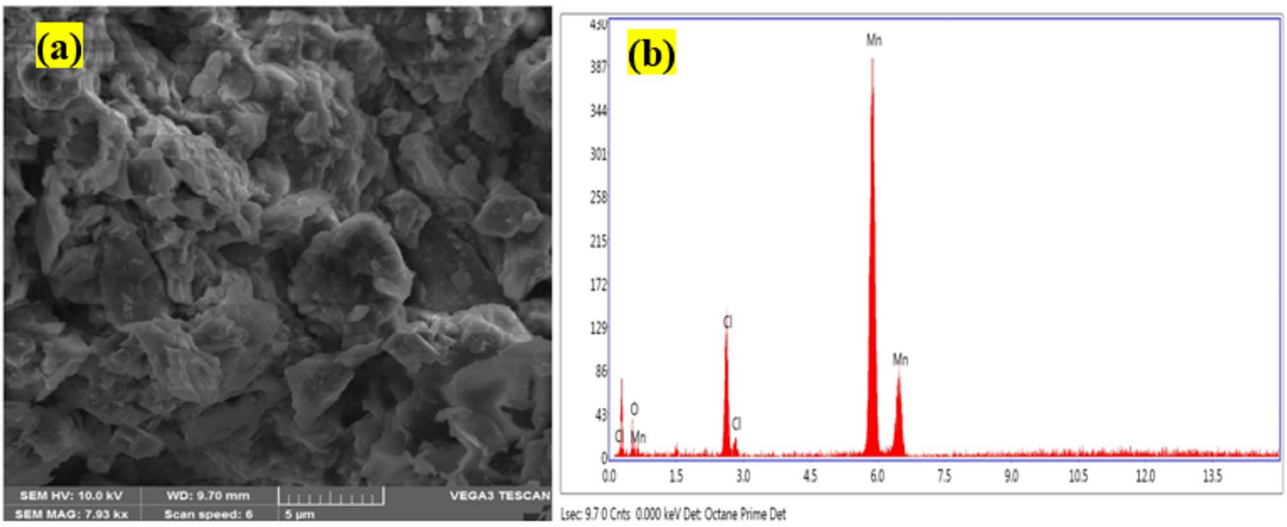

Fig. 4. (**a**) SEM image of Manganese oxide (MnO_2) nano particle (**b**) Edax spectrum of MnO_2.

$$\eta_{\mathrm{ELE}} = \frac{V_{\mathrm{mp}} I_{\mathrm{mp}}}{\dot{S}} = \frac{\dot{E}_{\mathrm{el}}}{\dot{S}} \tag{3}$$

Where, outlet electrical power ($\dot{E}_{\mathrm{el}}$) and the rate of solar energy incident on the PV surface ($\dot{S}$) is given by[6].

$$\dot{S} = G N_s N_m A_{\mathrm{mod}} \tag{4}$$

N_m and N_s are number of modules in series per string and number of strings, respectively. PV module area (A_{mod}) is given by

$$A_{\mathrm{mod}} = L_1 L_2 \tag{5}$$

Where, L_1 and L_2 are the length of PV module and the width of PV module, respectively.

Thermal exergy calculations

The thermal energy carried by the coolant has a lower exergy value than its energy content. It is calculated based on the Carnot efficiency[8].

$$\dot{E}x_{th} = \dot{m}\, C_p \left[(T_{out} - T_{in}) - T_a \ln \left(\frac{T_{out}}{T_{in}} \right) \right] \tag{6}$$

The overall exergy produced by the PVT system is the sum of its electrical and thermal exergy output[11].

$$\dot{E}x_{out} = \dot{E}x_{th} + \dot{E}x_{el} \tag{7}$$

The exergy destruction or the irreversibility may be expressed as follows:

$$\dot{E}x_{iire} = T_a\, \dot{S}_{gen} \tag{8}$$

$$\dot{S}_{gen} = \dot{m} C_p \ln \frac{T_{out}}{T_{in}} - \frac{\dot{Q}_s}{T_s} + \frac{Q_0}{T_a} \tag{9}$$

$$Q_0 = \dot{Q}_s - \dot{m} C_p \left(T_{out} - T_{in} \right) \tag{10}$$

The exergy efficiency or second law efficiency may be expressed as follows:

$$\eta_{EX} = 1 - \frac{T_a\ \dot{S}_{gen}}{\left[1 - (T_a / T_s) \right] \dot{Q}_s} \tag{11}$$

Statistical analysis

The correlated factor (r) and root mean square percentile deviation (e) have been computed using the following formulas in order to compare simulated and experimental data[44].

$$e_i = \frac{X_i - Y_i}{X_i} \mathrm{X}\, 100 \tag{12}$$

$$r = \frac{n \left(\Sigma\, X_i \mathrm{X}\, Y_i \right) - \left(\Sigma\, X_i \right) \left(\Sigma\, Y_i \right)}{\sqrt{n\, \Sigma\, X_i^2 - \left(\Sigma\, X_i \right)^2} \sqrt{n\, \Sigma\, Y_i^2 - \left(\Sigma\, Y_i \right)^2}} \tag{13}$$

$$e = \sqrt{\frac{\Sigma \left(e_i \right)^2}{n}} \tag{14}$$

In equations, n is the number of samples present in the data, and X and Y stand for experimental and simulated data sets, respectively.

Uncertainty error analysis

Numerous instruments, including a sensor for temperature, wind direction sensor, solari meter, mass, moisture ration and relative humidity, are part of the experimental setup. Key parameters and its minimum error values is displayed in Table 3. The following formulas are provided below to compute the degree of uncertainty and evaluation of errors[45].

$$S_x = \left[\frac{1}{N-1} \sum \left(X_i - \overline{X} \right)^2 \right]^{\frac{1}{2}} \tag{15}$$

Description	Error
Ambient air temperature	± 1 °C
Anemometer	±0.1 m/s
Cup anemometer	± 2%
Glazing surface temperature	± 1 °C
inlet air channel temperature	± 1 °C
outlet air channel temperature	± 1 °C
PV test circuit	± 1%
Voltmeter	± 1 V
Ammeter	± 1 amps
Wind speed	± 1 m/s
Wind vane	± 0.3

Table 3. Key parameters and its minimum error values.

Factor	Training Set			Testing Set			Total		
	S1	S2	S3	S1	S2	S3	S1	S2	S3
Power Output	1.08	2.18	0.96	1.58	3.42	0.97	1.36	2.59	0.98
Ele. Eff.	32.68	3.58	0.96	33.69	5.67	0.92	33.96	4.52	0.94

Table 4. Multilayer perceptron (MLP) model.

Factor	Training Set			Testing Set			Total		
	S1	S2	S3	S1	S2	S3	S1	S2	S3
Power Output	1.03	1.79	0.95	1.05	1.87	0.96	1.06	1.89	0.97
Ele. Eff.	32.43	3.27	0.97	33.17	3.58	0.97	33.26	3.52	0.96

Table 5. Radial basis neuron model.

The result t = 2.365 is obtained by using the t-distribution table with v = N − 1 = 7 degrees of freedom at the level of confidence of 95%.

$$P_x = t\,S_x \tag{16}$$

$$P_{\overline{X}} = \frac{t\,S_x}{\sqrt{N}} \tag{17}$$

Machine learning models

The PVT system's experimental data was split into training and testing sets at random. This work utilized a [80% / 20%] split, with [80%] of the dataset going towards training the models and [20%] set aside for independent testing to assess how well the models generalised to new data. This exacting division guarantees that the accuracy measures (RMSE, MAPE, and R2) supplied for the testing set accurately represent how well the model performs on fresh data. During the training stage, we used k-fold cross-validation to guarantee the stability of our models and reduce the possibility of overfitting. This entailed dividing the training data into 'k' equal subsets, using 'k-1' subsets for training and one subset for validation, then repeating the procedure 'k' times. A more accurate measure of the model's performance was given by the average performance over these folds.

For each machine learning model, including the Multilayer Perceptron (MLP), hyperparameter tweaking was methodically carried out to get maximum performance. One crucial hyperparameter was the number of neurones in the hidden layer. According on the performance metrics in Table 4, we methodically changed the number of hidden layer neurones from 5 to 20 to find the setup that produced the highest accuracy and computing efficiency. An important tuning parameter for the Radial Basis Function (RBF) model was the spread parameter (σi). The ideal network structure, which has a big influence on the model's capacity to approximation nonlinear functions, was found by varying this value between 0.1 and 1. Based on the accuracy findings in Table 4, the optimal structure was chosen. Forest Random (RF) Model: Parameters including the number of decision trees in the forest and the maximum depth of each tree were optimised as part of the Random Forest model's tuning process. To improve prediction accuracy and reduce overfitting, these parameters were changed, as shown in Table 5.

4Model of multilayer perceptron (MLP)

One type of feedforward artificial neural network (ANN) is the Multilayer Perceptron (MLP). An input layer, one or more hidden layers, and an output layer are the minimum number of node layers that make up this system. Every node is a neurone that employs a nonlinear activation function, with the exception of the input nodes. MLP trains via backpropagation, a supervised learning approach. MLP differs from a linear perceptron because to its numerous layers and non-linear activation. Data that is not linearly separable can be distinguished by it. The fundamental structure of MLP consists of three types of layers. The input layer is the layer that accepts the input characteristics. A characteristic of the incoming data is represented by each node in this layer[46].

The first layer may be thought of as a set of M dynamic neurones, which captures the core of mathematics. The terminal layer of neurone O1, k1, is articulated in Ref[47]. after the k1-th neurone receives the input xi.

$$o_{1,k_1} = f\left(\sum_{m=0}^{M} w_{mk1}\,x_m\right),\ k_1 = 1, \ldots,\ K_1 \tag{18}$$

The findings can then be used as input for the concealed layer. All neural networks in the invisible layer provide the following output:

$$oh,\ kh\ =\ \varphi\left(\sum_{K_{h-1}=0}^{K_{h-1}} w_{K_{h-1},k_h}\, o_{h-1,k_{h-1}}\right),\ k_h\ =\ 1,\ ...,k_h,\ h\ =\ 1,\ ...,\ N_h \tag{19}$$

w0, kh, kh = 1,., and Kh stand for the input parameters and submerged layer biases, respectively, and φ for the activation function. The symbols wkm, kh stand for the input and unseen layer weights. The values of the inputs and the hth hidden layer neurones are denoted by M and Kh. The number of hidden layers is denoted by Nh. One may calculate the output neurone as follows:[48]

$$y_1\ =\ \sum_{K_N=0}^{K_N} w_{kh,l}\, o_{h,k_h} k_h = 1, ..., K_h \tag{20}$$

In this equation, L refers to the neurones in the output layer, whereas wkh, l, kh = 1,…, Kh represent the link weights that can discard neurones in the concealed and yield layers. The multilayer perceptron model's training, testing, and total sets of three accuracy predictions RMSE as S1, MAPE as S2, and R2 as S3 can be carried out by power output and electrical efficiency, and three sets of datas were plotted in Table 4. The process table for MLP model is shown in Fig. 5.

Radial basis function (RBF) model

In machine learning, numerical analysis, and function interpolation, a Radial Basis Function (RBF) model is a form of function approximation model that is frequently utilised. In neural networks, kernel techniques, and spatial interpolation, it is heavily utilised and especially helpful for approximating nonlinear functions. RBF models divide themselves into three levels: input, hidden, and output. From the input layer, data is received. RBF activation functions are used by the buried layer to map the input data non-linearly. The output layer uses a weighted sum to create a scalar function from the input vector. Power output and electrical efficiency may be used to train, test, and determine the overall sets of three accuracy predictions (RMSE, MAPE, and R2) for the radial basis function model, as shown in Table 5. Neural networks in the hidden layer of the RBF technique are arranged according to a nonlinear activation function. One may calculate the output of the RBF model as[49].

$$Y\ =\ W^T\phi\ =\ \sum_{j=1}^{L_2} w_{ij}\varphi(||x\ -\ c_i||) \tag{21}$$

W_{ij} crosses the layer that is concealed to the output, L_2 is the invisible layer neurones, c_i is the centre of the neurones in the invisible layer,

$$\varphi_i\,(x)\ =\ \exp\left(\frac{||x\ -\ c_i||^2}{\sigma_i^2}\right) \tag{22}$$

σi is the spread factor. In this investigation, the spread parameter was adjusted from 0.1 to 1 to find the best network structure. There are several methods for training a network and correcting the temperature to achieve a substantial inaccuracy in an RBF model. Perhaps the most used ways is the flawed BP algorithm[49], which was applied in this work. Each ideal incessant gathering in the Artificial Neural Network model may be represented by a concealed layer comprising an appropriate number of neurones. As a result, the RBF and MLP models are treated as having one concealed layer in this investigation. The viability of the RBF and MLP models was tested by varying the number of neurones in the hidden layer from 5 to 20, and the best structure was chosen for modelling. As a result, at the output layer, this study employed transfer equations for the RBF and MLP models. The process table for RBF model is shown in Fig. 6.

The RBF networks are especially well-suited for modelling the intricate, non-linear connections found in the data from our PVT system, as we have explained. Intricate patterns that may be more difficult for global approximators like regular MLPs without substantial tuning or deeper architectures to catch are frequently captured by RBFs due to their localised activation functions and capacity to generate "local experts" in the feature space. The effectiveness of RBF indicates that our input parameters (such as flow rate, ambient temperature, and solar radiation) and output (such as power output and electrical efficiency) probably have highly non-linear and localised correlations. The residuals (prediction errors) of each model may be visually or statistically analysed to demonstrate how RBF's mistakes are more consistently distributed and lower, suggesting a better fit over the data range. Talking about Model Complexity vs. Performance: We may talk about the trade-off between model complexity and performance, showing that RBF, with its spread parameter and hidden layer neurones optimised, identified a more effective representation of the underlying structure of the data for our particular situation.

Random forest model

Several decision trees are combined in Random Forest, a flexible and popular ensemble learning technique, to enhance prediction accuracy and reduce overfitting. The main ideas, principles, and recommended procedures for comprehending and using Random Forests are listed here. A random subset of the data and features is used to train each decision tree in the random forest ensemble. A bootstrapped sample of the training data random sampling with replacement is used to train each tree. Only a random subset of characteristics is taken into account at each split in a decision tree, which improves generalisation and decreases correlation between trees.

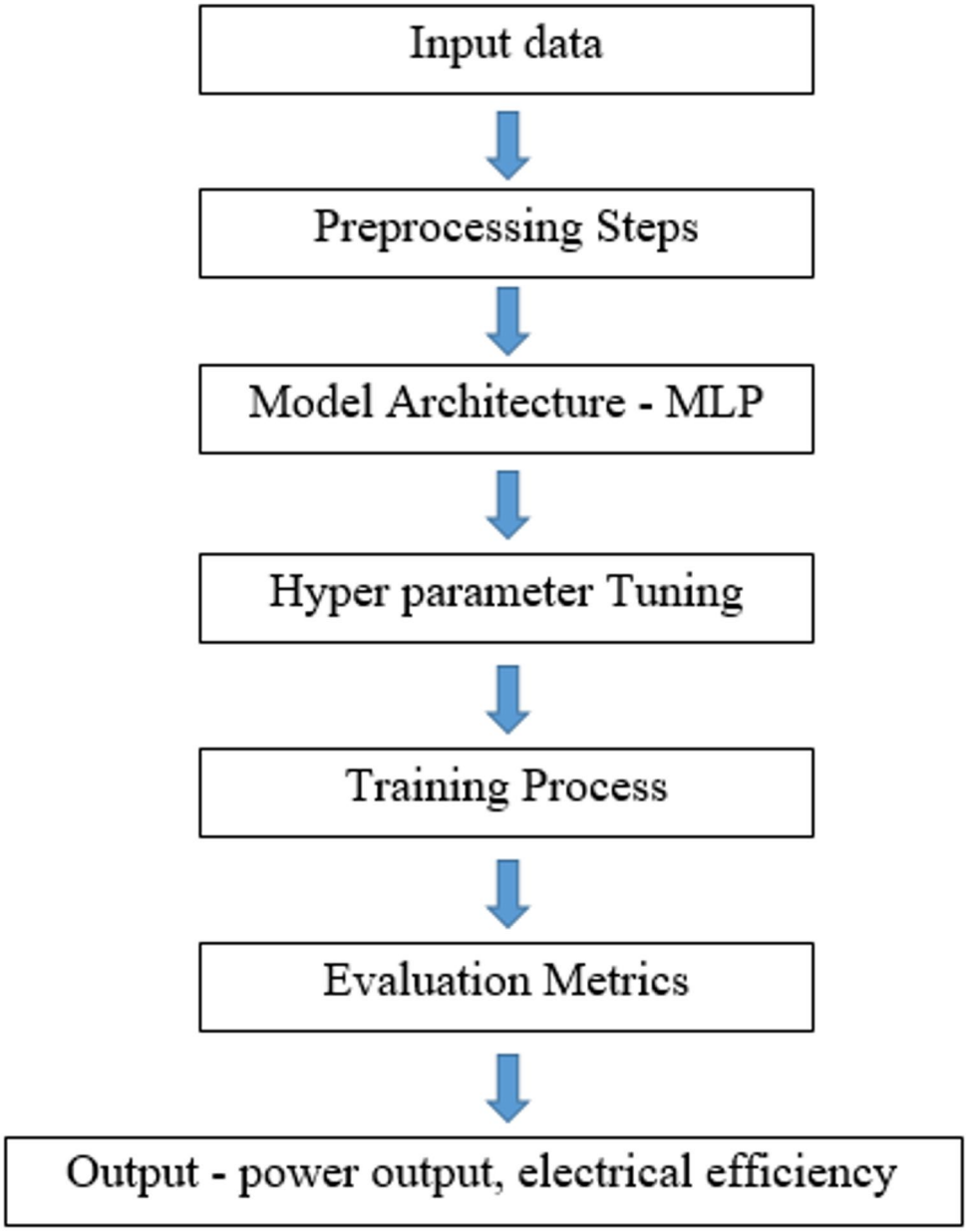

Fig. 5. The process table for MLP model.

Three kinds of accuracies and training, testing and total sets of temperature dryness and mass dryness is shown in Table 6. The process table for RF model is shown in Fig. 7.

Performance criteria evaluation

The MLP, RBF, and RF algorithms for forecasting the temperature and mass of dried red chillies were assessed in this work using a variety of performance metrics, including as RMSE, MAPE, and R^2[48,50].

$$RMSE \sqrt{\frac{\sum_{j=1}^{n} (T_{dj} - T_{pj})^2}{n}} \tag{23}$$

$$MAPE = \frac{1}{n} \sum_{j=1}^{n} \left| \frac{T_{dj} - T_{pj}}{T_{dj}} \right| X\ 100 \tag{24}$$

$$R^2 = \left[\frac{\sum_{j=1}^{n} \left(T_{dj} - \overline{Td}\right) \left(T_{pj} - \overline{Td}\right)}{\sum_{j=1}^{n} \left(T_{dj} - \overline{Td}\right) X \sum_{j=1}^{n} \left(T_{pj} - \overline{Td}\right)} \right]^2 \tag{25}$$

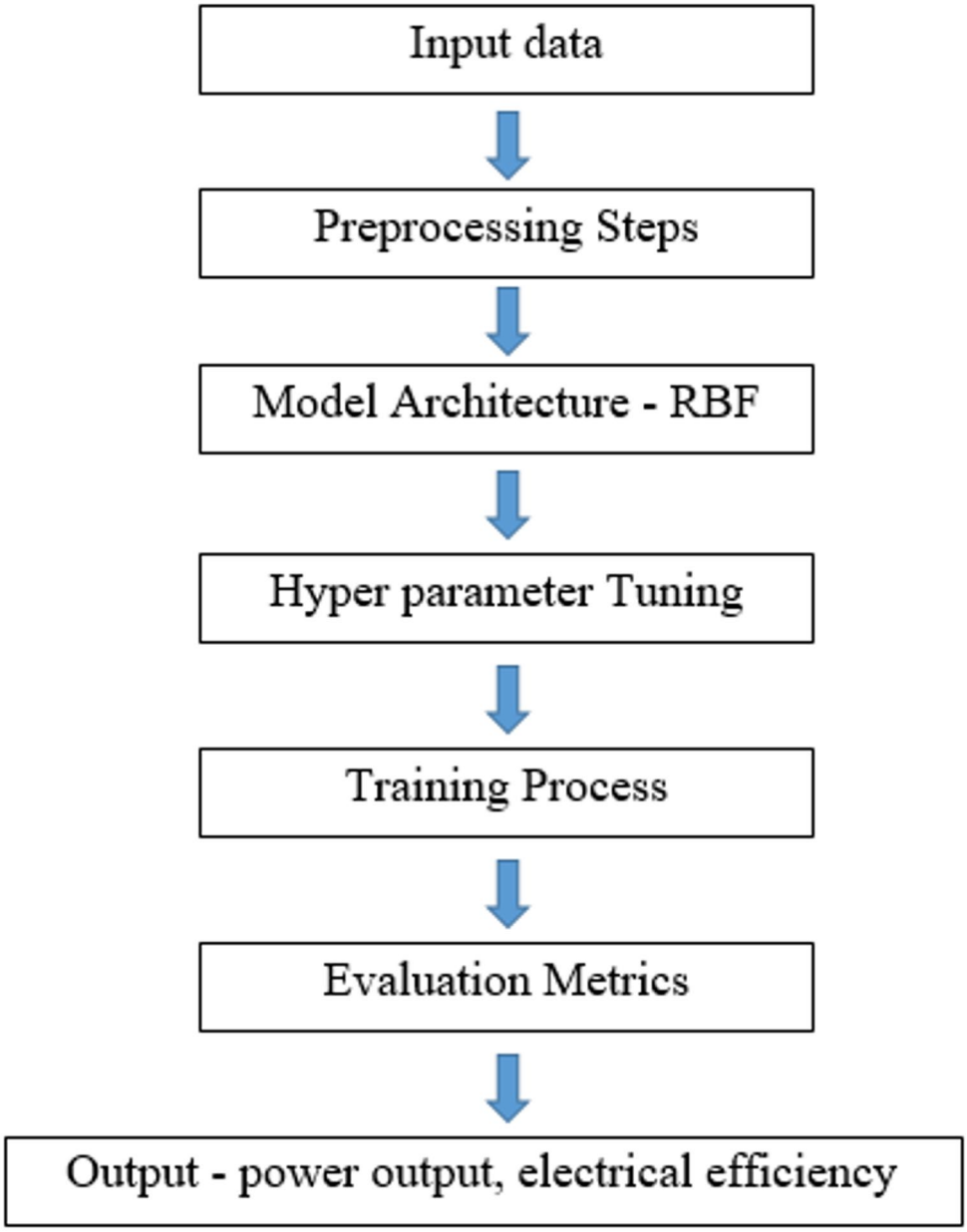

Fig. 6. The process table for RBF model.

Factor	Training Set			Testing Set			Total		
	S1	S2	S3	S1	S2	S3	S1	S2	S3
Power Output	1.69	3.78	0.87	2.29	4.28	0.91	1.88	3.45	0.95
Ele. Eff.	38.23	48.91	0.62	39.21	47.23	0.82	98.45	50.12	0.56

Table 6. *Random forest* (RF) model.

Results and discussion

This work deals with the three kinds of testes were carried out for the performances of PV and PVT collector. The independent PV system, water PVT and water based MnO_2 Nano fluid PVT collector. An independent PV system has no cooling channel which is ideal conditions as well as comparative study of both water PVT collector and water based PVT collector. Various parametric studies deal with this article namely glazing surface temperature, tedlar surface temperature, power output of the PV and PVT collector, solar radiation, ambient temperature, current and voltage of the concern panel. In addition to that experimental electrical efficiency can be evaluated by machine learning models.

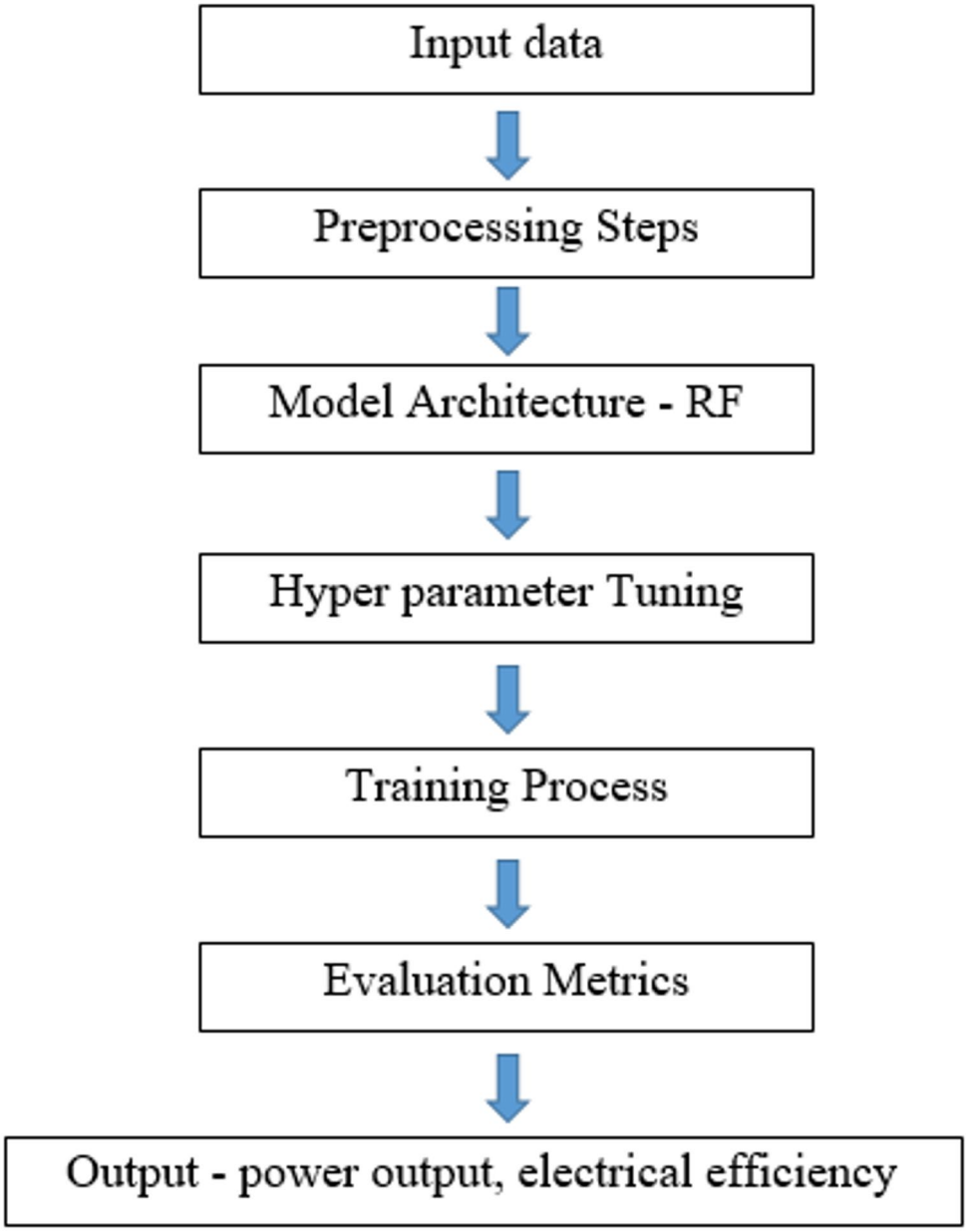

Fig. 7. The process table for RF model.

An hourly variation of an average values of output power and other parameters of all the three systems were displayed in Fig. 8. An independent PV system has nil cooling unit which consists of solar panel which can be generated electrical power since morning to evening of the test days. The voltage and current were directly depend on the amount of incidental solar radiation on the collector surface and also ambient temperature were linearly linked with solar radiations. As per the given figure above it states that maximum voltage can be attained by noon of the day about 26.48 V, and similarly current 5.50 Amps got maximum at midday of the test day. Further, solar radiation and ambient temperature were also attained maximum during the midday of the test days which were about 1008 W/m2 and 33.66 °C. This study investigates the three kinds of flow rates of water and water based nano fluids which also evaluated by machine learning models whereas the other study[51] was done an experimental analysis of TiO_2 along with water and water based nano fluids which were evaluated by earlier literatures. The present study and previous study were significantly agreed with each other in their aspects of performances.

An hourly variations of glazing surface and tedlar surface temperature, power output of the solar PVT collector and electrical efficiency were shown in Fig. 9. The glazing surface temperature is also known as top surface of the solar panel. Thermocouples that recorded the temperature in a data logger were used to measure the surface temperature of solar panels or glass. The temperature of the solar panel's glazing will rise as sunlight strikes it, and this temperature is transferred to the tedlar side, which is the rear of the panel. Thermocouples attached to a

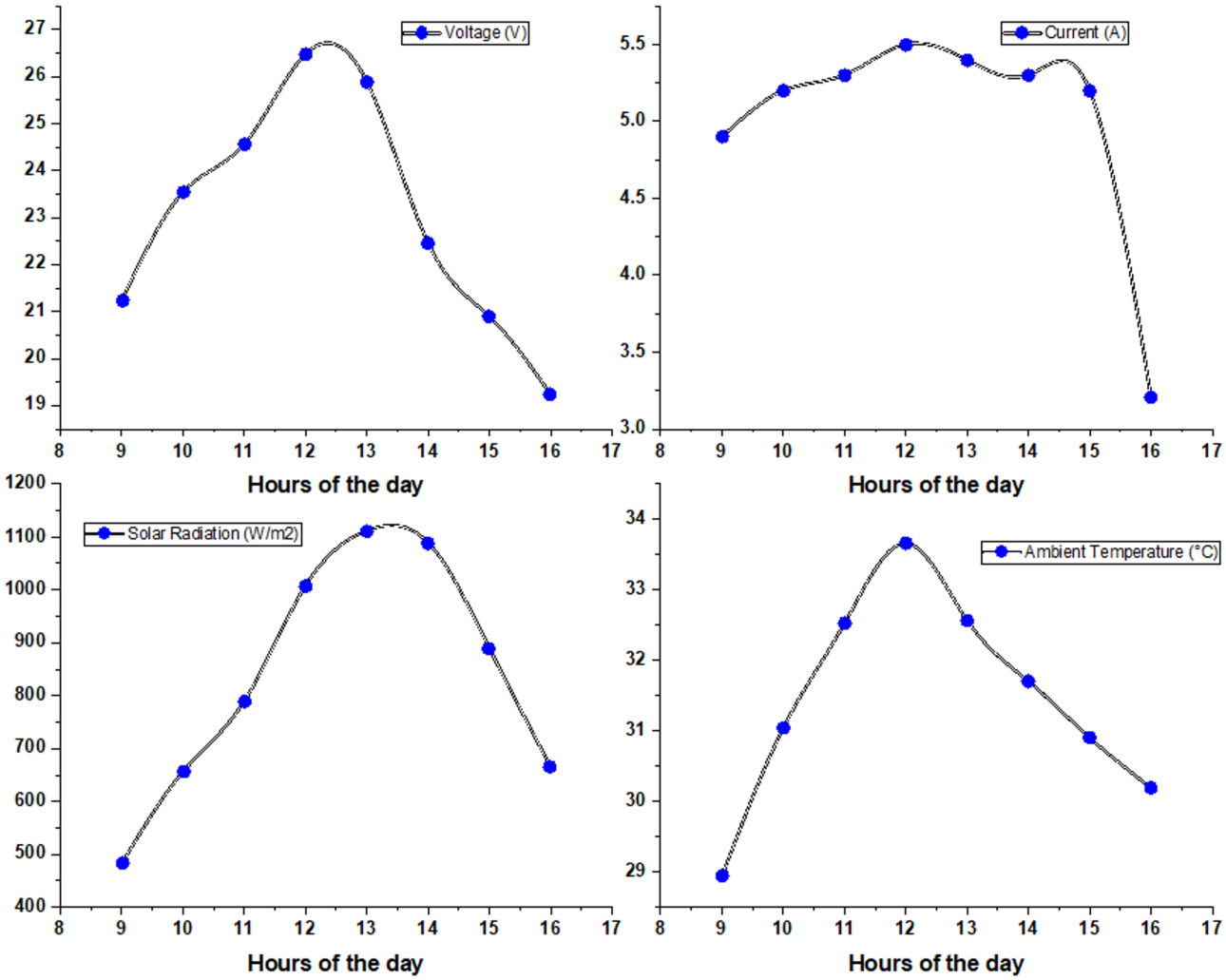

Fig. 8. The average values of output power and other parameters of all the three systems.

data recorder were also used to measure the temperature on the teddy side. While convective heat transmission happened over a tedlar surface, conduction heat transfer occurs in a glazed surface. As mentioned earlier in this article that an independent system had no cooling provisions which lead high amount of glazing, tedlar surface temperatures. In contrast, low amount of power generation and poor electrical efficiency. Comparable conclusions were discovered in[52].

An hourly variations of glazing surface and tedlar surface temperature, power output of the solar PVT collector and electrical efficiency were demonstrated in Fig. 10. Water is a better coolant than air as a medium of cooling because water has high heat carrying capacity which is about 4.18 kJ/kg·K. This absorbs and retains the heat efficiently and also helps the transfer of heat from the tedlar side of the solar panel. In addition to that cost effective and free usage however it has own demerits as less corrosion resistant.

An hourly variations of glazing surface and tedlar surface temperature, power output of the solar PVT collector and electrical efficiency were presented in Fig. 11. The glazing surface temperature and electrical efficiencies were indirectly proportional which was given by the above figure. While convective heat transmission happened over a tedlar surface, conduction heat transfer occurs in a glazed surface. The electrical efficiency was 6.23% when the glazing surface temperature was 62.28 °C. At the same time, the tedlar surface temperature and glazing surface temperature moved linearly throughout the day. Additionally, the power generation in watts is approximately 172.56 W depending on the heat removal from the back side of the solar panel that was achieved, whether it was poor or better. Comparable conclusions were discovered in[53,54].

An hourly variations of glazing surface and tedlar surface temperature, power output of the solar PVT collector and electrical efficiency were displayed in Fig. 12. Since a tedlar surface is closed, its temperature was always higher than that of the glazing. Moreover, higher-temperature ambient air travels over the tedlar side, which adds to the tedlar temperature increase. The glazed surface, however, is exposed to the environment and gets wind, both of which lower the surface temperature. When the glazing surface temperature was 63.55 °C, the electrical efficiency was 5.82%. Simultaneously, the glazing and tedlar surface temperatures increased linearly

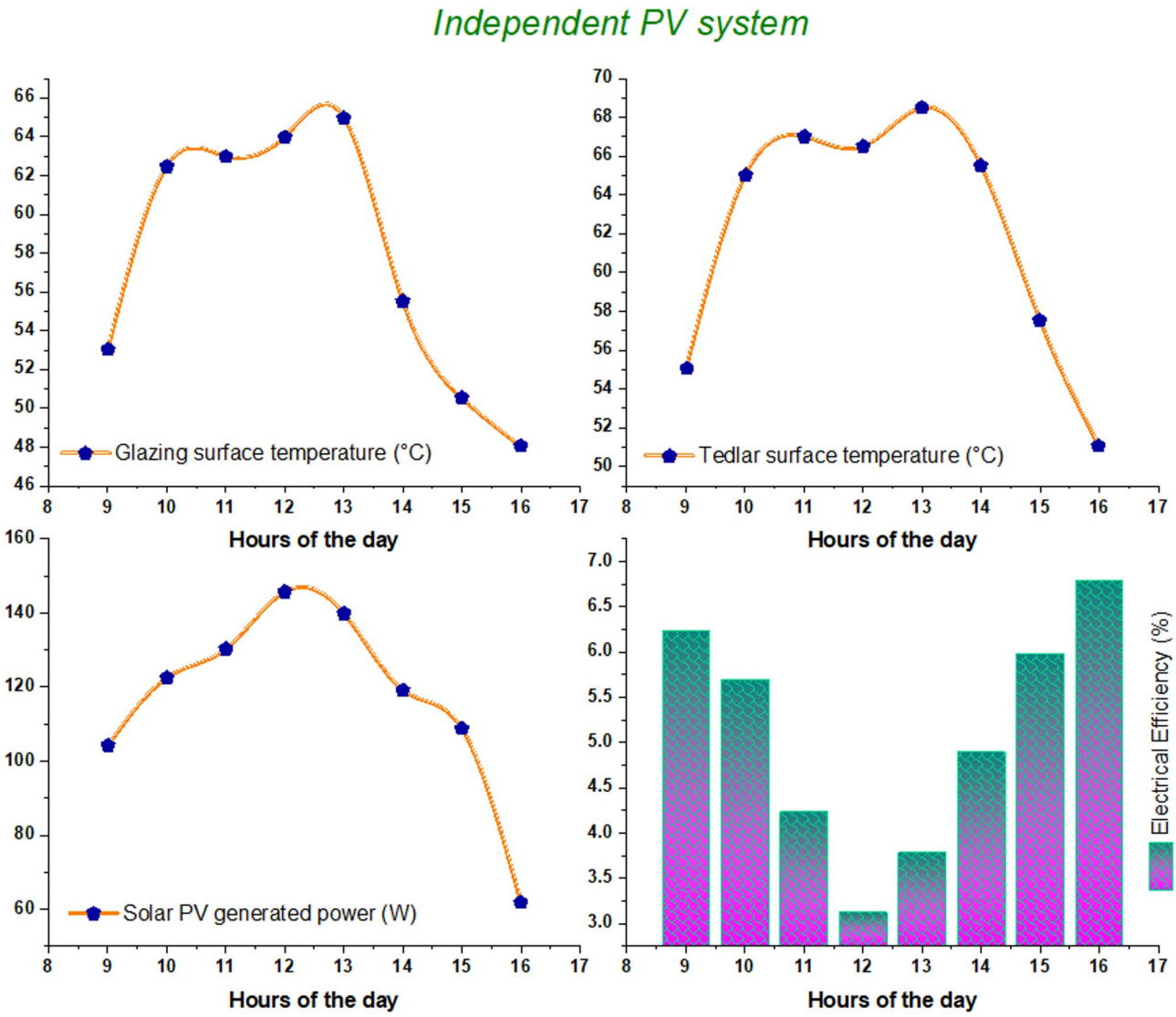

Fig. 9. Various data of Independent PV system.

over the day. The morning and evening hours of the day had relatively lower power generation, with around 119.56 W and 72.48 W, respectively. Results identical to these were found in[55,56].

The hourly variations of present study namely 0.5, 1.0 and 1.5 LPM of water and its cell temperature along with case A and case B of Tiwari and Al-Helal 2015 with its cell temperatures were plotted on Fig. 13[57]. The present study consists of three kinds of water flow which were mentioned above which can be justified through two kinds of cases namely case A and case B from the respected figure. In general cell temperature linearly dependent on electrical efficiency. As cell temperatures were increased the electrical efficiency dropped and vice versa which can be shown since morning to evening of the experimental days[58]. Although both studies exhibit the expected diurnal trend of photovoltaic (PV) cell temperature—rising from morning to midday and declining towards the evening—significant differences in temperature magnitude are observed. Notably, the cell temperatures recorded in the present investigation are consistently higher than those reported by Tiwari and Al-Helal (2015) for both Case A and Case B, particularly at water flow rates of 0.5, 1.0, and 1.5 LPM. While Tiwari and Al-Helal observed peak midday cell temperatures of approximately 45 °C and 47 °C for Case A and Case B, respectively, our study recorded a considerably higher temperature nearing 60 °C at a flow rate of 0.5 LPM around 13:00 h.

These discrepancies may be attributed to several key factors. First, geographical and climatic conditions play a crucial role. Our experiments were conducted in Chennai, India, during June and July 2024—a period characterized by intense solar irradiation and prolonged sunshine. Variations in ambient temperature, solar radiation intensity, and wind speed between Chennai and the location of Tiwari and Al-Helal's study likely influenced the thermal behavior of the PV panels. Even slight environmental differences can significantly affect PVT system performance. Second, system design and component differences can contribute to variation. While both studies utilized PVT systems, differences in PV module type, absorber plate design, material selection,

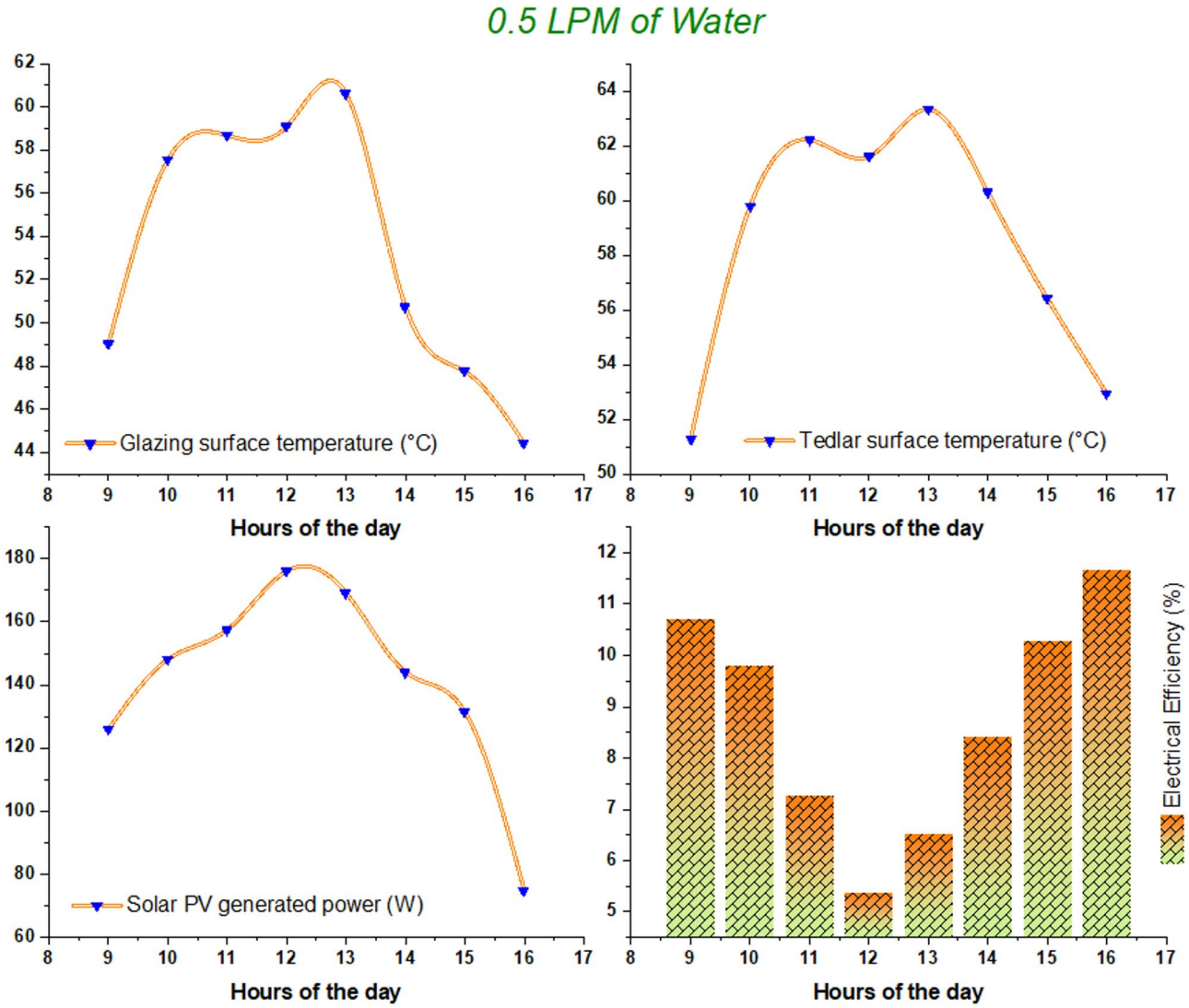

Fig. 10. Various data of 0.5 LPM of water PVT Collector.

and cooling channel configuration can result in distinct heat transfer characteristics. In our study, we employed a specific multi-silicon PV module (Model No. AE689VBN1254, Panasonic), which may contribute to the observed temperature differences. Third, variability in experimental setup and instrumentation could influence the results. Differences in measurement techniques, sensor calibration, and instrumentation accuracy—such as flow meters, temperature sensors, and solarimeters—may introduce additional discrepancies between the studies.

Despite these variations, the qualitative agreement in the overall hourly temperature profile provides a meaningful basis for comparison. The higher cell temperatures recorded in our conventional water-cooled PVT system underscore the need for more effective thermal management strategies. In response, the subsequent sections of our study explore the integration of water-based MnO_2 nanofluids as an advanced cooling solution. Additionally, the application of machine learning (ML) models—specifically Multilayer Perceptron (MLP), Radial Basis Function (RBF), and Random Forest (RF)—enabled accurate prediction of power output and electrical efficiency based on experimental data. Among them, the RBF model achieved the highest predictive accuracy, with R^2 values of 0.96 and 0.97 for power and efficiency, respectively, on the testing dataset. This strong correlation between experimental and predicted values validates the effectiveness of our ML approach and confirms its capability to capture complex, non-linear relationships inherent in PVT system behavior.

In addition to case A and case B with their electrical efficiency of Tiwari and Al-Helal 2015, Fig. 14[41], displayed the hourly fluctuations of the current investigation, namely 0.5, 1.0, and 1.5 LPM of water and its electrical efficiency. Using Eq. 1 through 5, the electrical efficiency was calculated and shown on the graph above. Due to the fact that cell temperature essentially influences solar radiation and ambient temperatures at the specific site on the day of the experiment, the electrical efficiencies were extremely reactive. By these standards, electricity efficiency has taken action[59]. Figure 13 clearly indicates that the electrical efficiencies reported by Tiwari and Al-Helal (2015) for both Case A and Case B are generally higher than those observed in the present

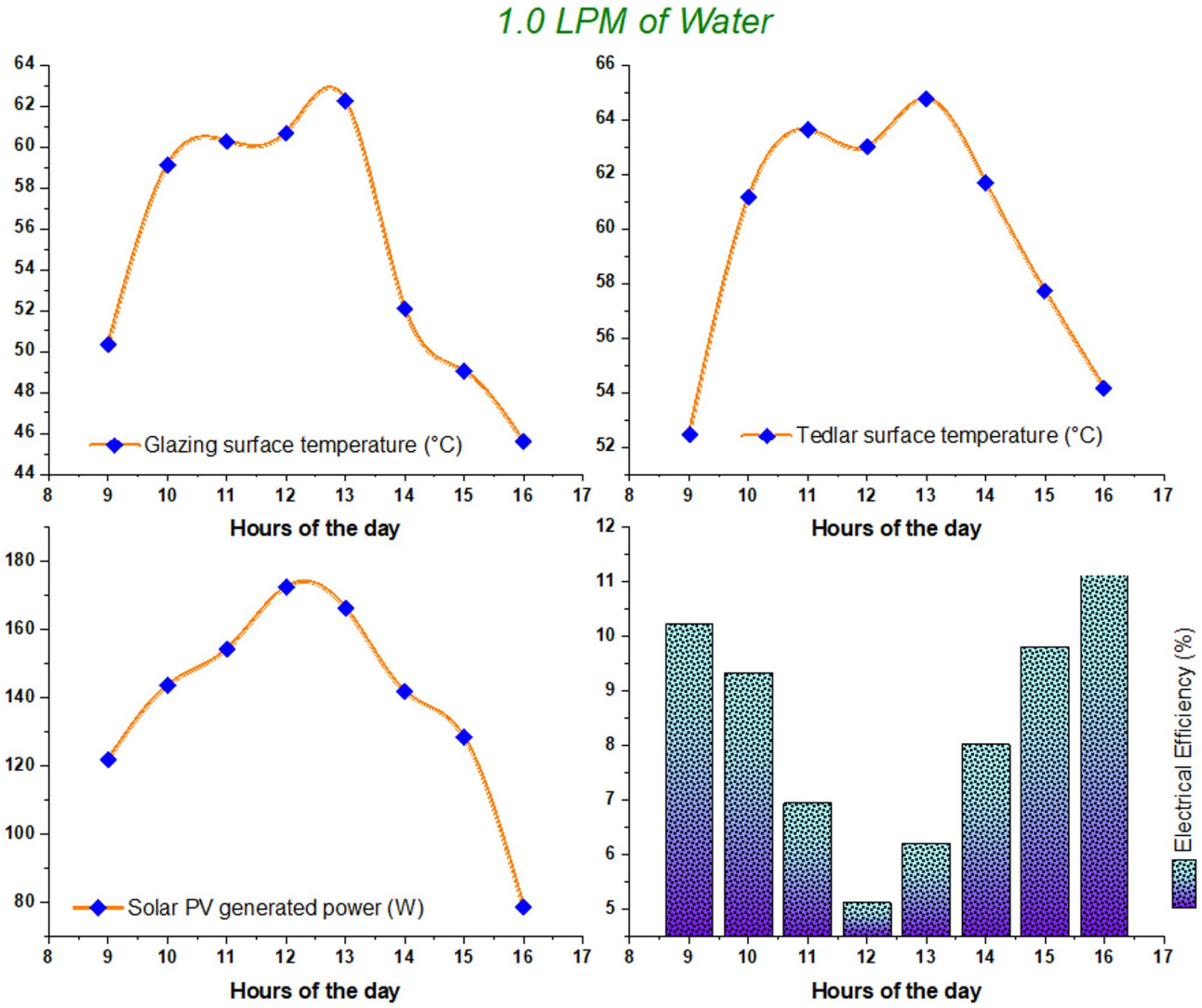

Fig. 11. Various data of 1.0 of LPM of water PVT Collector.

study, particularly during most hours of the day. For example, at 9:00 AM, Case A and Case B exhibited electrical efficiencies of approximately 14.5% and 14.2%, respectively. In contrast, the water-cooled PVT system evaluated in our investigation demonstrated lower efficiencies, ranging from about 10% to 10.5% across the different flow rates. This trend of comparatively reduced electrical efficiency persists consistently throughout the day in our experimental results when compared to the referenced study.

The observed discrepancies in electrical efficiency between our study and that of Tiwari and Al-Helal (2015) can be attributed to several factors. First, site-specific environmental conditions play a critical role. Our experiments were conducted in June and July 2024 in Chennai, India, a region characterized by high ambient temperatures, variable wind speeds, and specific solar radiation levels. These environmental parameters significantly influence photovoltaic performance. Higher ambient temperatures and potentially lower solar irradiance at our test location could elevate cell temperatures, thereby reducing electrical efficiency compared to the conditions reported in the reference study. Second, differences in PV module characteristics may also account for the variations. Even when using similar PVT system concepts, the specific properties of the PV module—such as nominal efficiency, temperature coefficient, and material composition—can influence performance. In our case, a Panasonic module with rated voltage at P_max of 30.9 V and current at P_max of 8.42 A was used. Disparities in these intrinsic electrical characteristics likely contributed to the observed differences in efficiency.

Third, variations in experimental setup and operational parameters may further affect system performance. While both studies utilized water as a cooling medium, differences in cooling channel geometry, flow paths, or heat exchanger design can impact heat removal efficiency and, consequently, electrical output. Our study specifically examined three flow rates (0.5, 1.0, and 1.5 LPM), which may differ from those employed in the referenced work. Despite these numerical differences, our findings reaffirm the well-established inverse relationship between PV cell temperature and electrical efficiency: as cell temperature increases, electrical efficiency decreases. This consistent trend, observed throughout our experimental trials, aligns with fundamental photovoltaic principles and underscores the importance of effective thermal management in PVT systems.

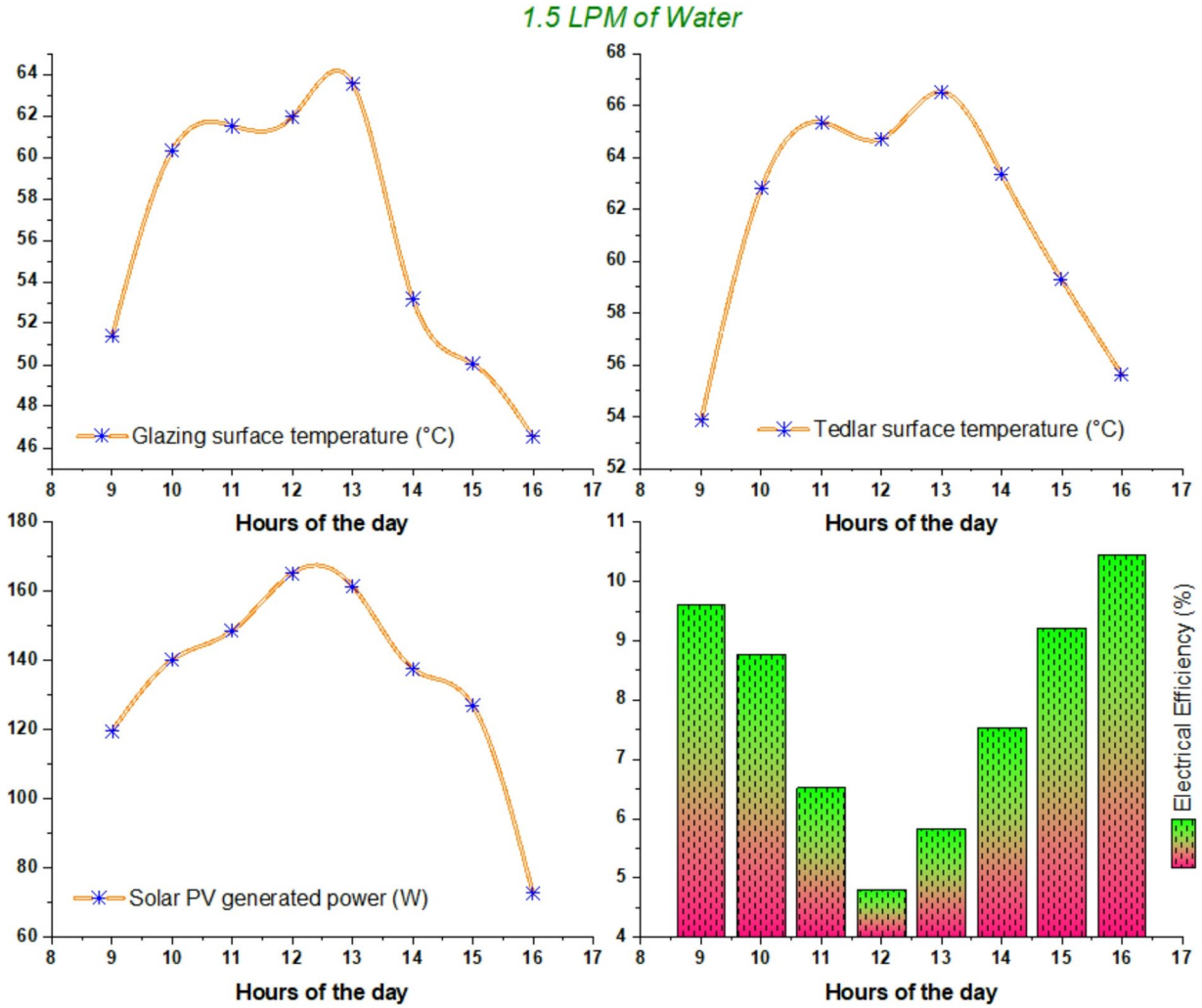

Fig. 12. Various data of 1.5 of LPM of water PVT Collector.

An hourly variations of glazing surface and tedlar surface temperature, power output of the solar PVT collector and electrical efficiency were exhibited in Fig. 15. As the temperature of the solar cells rises, PV panel efficiency falls. This is mostly because the bandgap and carrier recombination rates, among other characteristics of semiconductor materials, are temperature dependent. Electrical efficiency is decreased by excessive heat in PV panels; cooling systems such as nanofluids assist preserve peak performance. PVT collectors' cooling efficiency is increased by nanofluids, which are nanoparticles distributed in a base fluid and boost electrical performance. According to the above figure, the maximum temperatures for the glazing, tedlar, power output, and electrical efficiency are approximately 53.37 °C, 55.08 °C, 202.91 W, and 14.58%, respectively. Every parameter had improved with a varied time of day, namely the glazing surface temperature and the tedlar temperature at 1 pm. On the other hand, electrical efficiency was achieved by 4 p.m. on the day of the trial. While Al-Shamani et al.[60] used SiC nano fluid to get the best electrical efficiency of around 13.52%, our work used MnO_2 nano fluid to achieve the highest electrical efficiency of around 14.58% for 0.5 LPM of water base MnO_2 nano fluid.

The objective of this research is to enhance the performance of photovoltaic-thermal (PVT) collectors by integrating machine learning (ML) models and employing water-based manganese dioxide (MnO_2) nanofluids. To comprehensively characterize the system's behavior under varying operating conditions, experiments were conducted at three strategically selected water flow rates: 0.5, 1.0, and 1.5 LPM. This approach enabled the identification of flow-dependent thermal and electrical phenomena that would not be observable at a single flow rate. Such variation was essential for identifying optimal operating conditions and evaluating the system's reliability across a range of scenarios. To predict and optimize PVT performance, three ML models—Random Forest (RF), Radial Basis Function (RBF), and Multilayer Perceptron (MLP)—were developed and trained using experimentally obtained data. Hyperparameters for each model were carefully tuned, including the spread value for RBF and the number of neurons in the hidden layers of both RBF and MLP. The dataset was split into training and testing subsets to ensure robust validation.

Among the models, the RBF demonstrated the highest predictive accuracy, effectively capturing the complex, non-linear relationships present in the system's thermal and electrical performance data. While some differences

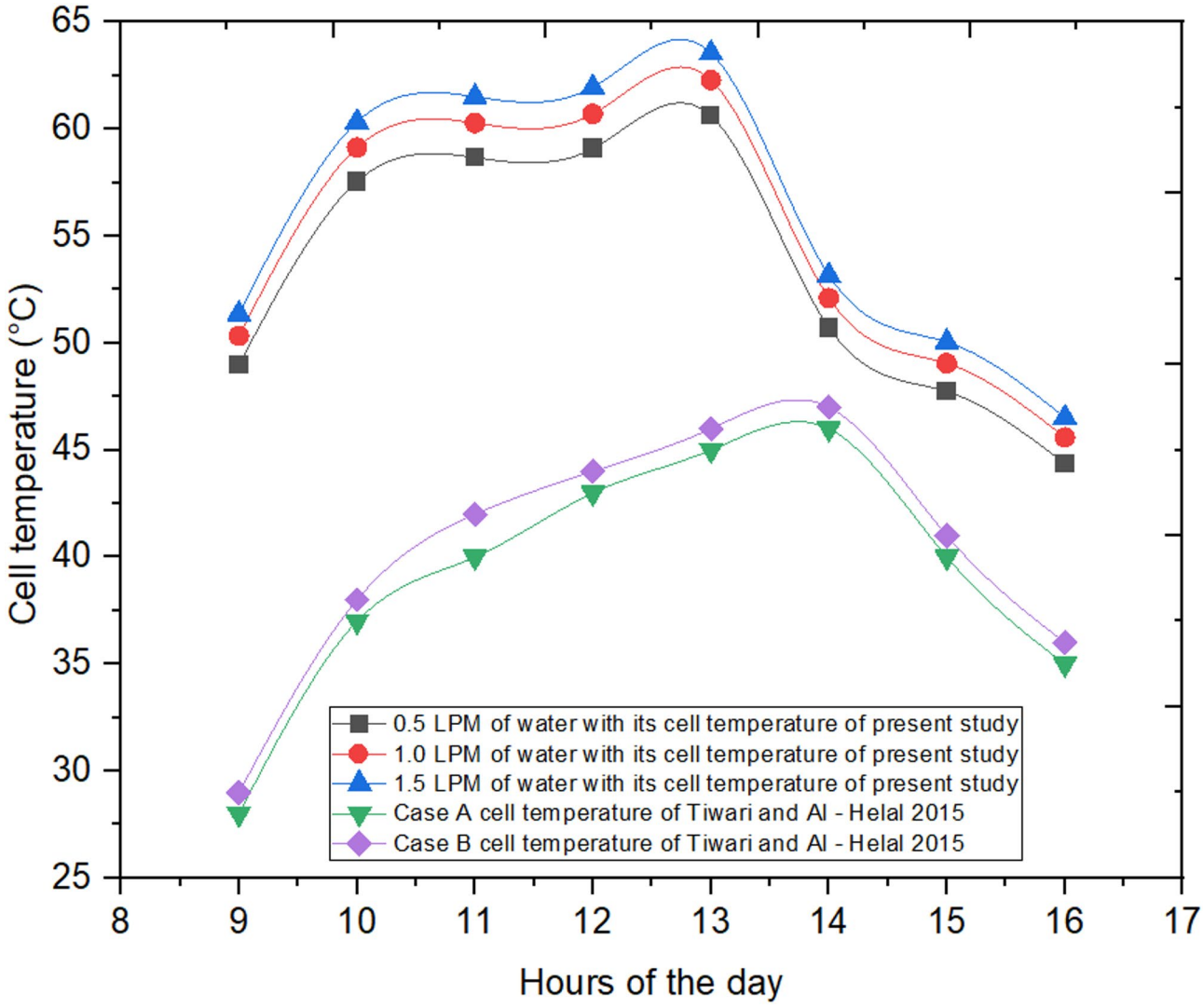

Fig. 13. The present study with Tiwari and Al – Helal 2015.

in cell temperature and electrical efficiency were observed compared to prior studies (e.g., Tiwari and Al-Helal, 2015), these were primarily attributable to differences in geographic and climatic conditions, system configurations, and experimental setups. Nonetheless, the observed trends remained consistent with well-established photovoltaic principles. The predictive capability of the proposed ML models was strongly validated against experimental results. The integration of MnO_2 nanofluids led to significant improvements, with electrical efficiencies reaching up to 14.58% and power output ranging from 80.42 W to 202.91 W, outperforming both conventional water-cooled PVT and standalone PV systems. These findings hold considerable practical relevance, suggesting potential for reduced energy costs, faster return on investment, improved space utilization, and alignment with sustainable energy goals. A critical analysis of the unique advantages offered by MnO_2 nanofluids, along with the impact of diurnal variations, further reinforces the significance and applicability of this work.

An hourly variations of glazing surface and tedlar surface temperature, power output of the solar PVT collector and electrical efficiency were demonstrated in Fig. 16. The temperature of the front glass is affected by wind speed, ambient temperature, and sun irradiation. The effectiveness of the solar cells may be decreased by greater heat transfer caused by higher glazing surface temperatures. The heat dissipation from the solar cells and the thermal characteristics of the materials both affect the backsheet temperature. Higher cell temperatures and decreased efficiency can result from inadequate heat dissipation. Analogous findings were found in[61]. The electrical efficiency was 7.94% when the glass surface temperature was 54.69 °C. At the same time, the surface temperatures of the tedlar and glazing rose linearly throughout the day. Power generation was comparatively lower in the morning and evening, at about 139.31 W and 82.41 W, respectively. Electrical efficiency during those hours was 14.24% at 4 p.m. and 13.08% at 9 a.m. In an experimental study by Hassan et al.[62], electrical efficiency was reached at about 14.3%. This article examined experimental investigations that used MnO2 at a flow rate of 1.0 LPM to achieve 14.24% electrical efficiency.

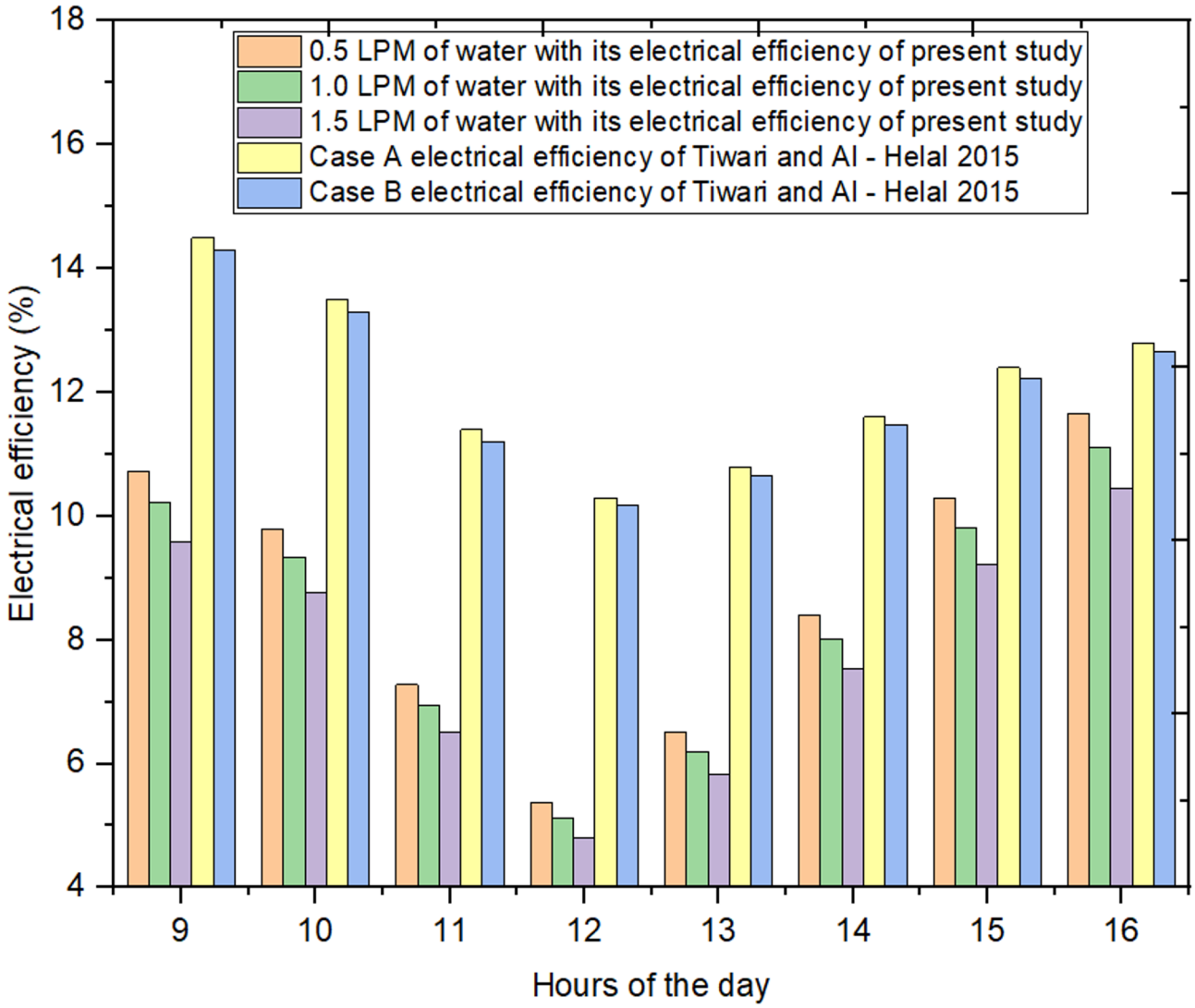

Fig. 14. The present study with Tiwari and Al – Helal 2015.

This study contributes to the ongoing discourse by critically analyzing the hourly fluctuations in system performance and their underlying causes. Particular attention is given to the influence of external environmental parameters—such as wind speed, ambient temperature, and solar irradiance—on the glazing and back surface (Tedlar) temperatures throughout the day. The analysis outlines how these surface temperatures typically increase linearly until solar noon and subsequently decline, and relates this thermal behavior to the corresponding hourly variations in electrical efficiency and power output. A specific focus is placed on interpreting the observed electrical efficiency of 7.94% at a glazing surface temperature of 54.69 °C. This is examined in light of the well-established inverse relationship between PV cell temperature and electrical performance, emphasizing how elevated glazing temperatures impair heat dissipation and consequently reduce electrical efficiency.

To further understand the dynamic response of the cooling system, this study investigates the conditions that led to the peak electrical efficiency of 14.24% at 4:00 p.m. and the comparatively high morning efficiency of 13.08% at 9:00 a.m. These occurrences correspond with lower ambient temperatures and transitional irradiance levels, indicating more favorable thermal conditions for PV operation during those periods. Moreover, a comparative evaluation is presented with the experimental work of Hassan et al.[62], who reported an electrical efficiency of approximately 14.3%. Although the MnO_2-based system in this study achieved a closely similar efficiency of 14.24% at a flow rate of 1.0 LPM, a detailed analysis is undertaken to examine the minor differences and similarities between the two results. This includes consideration of variations in experimental setups, PV module characteristics, nanofluid concentrations, geographic locations, and environmental conditions.

An hourly variations of glazing surface and tedlar surface temperature, power output of the solar PVT collector and electrical efficiency were revealed in Fig. 17. Solar irradiance was the first of four important factors that affected the PVT collector's temperature and electrical performance. The PV panel's temperature and electrical output both rise with increased irradiation, with ambient temperature coming in second. Increasing panel temperatures result from a reduction in the cooling effect caused by increasing ambient temperatures. The

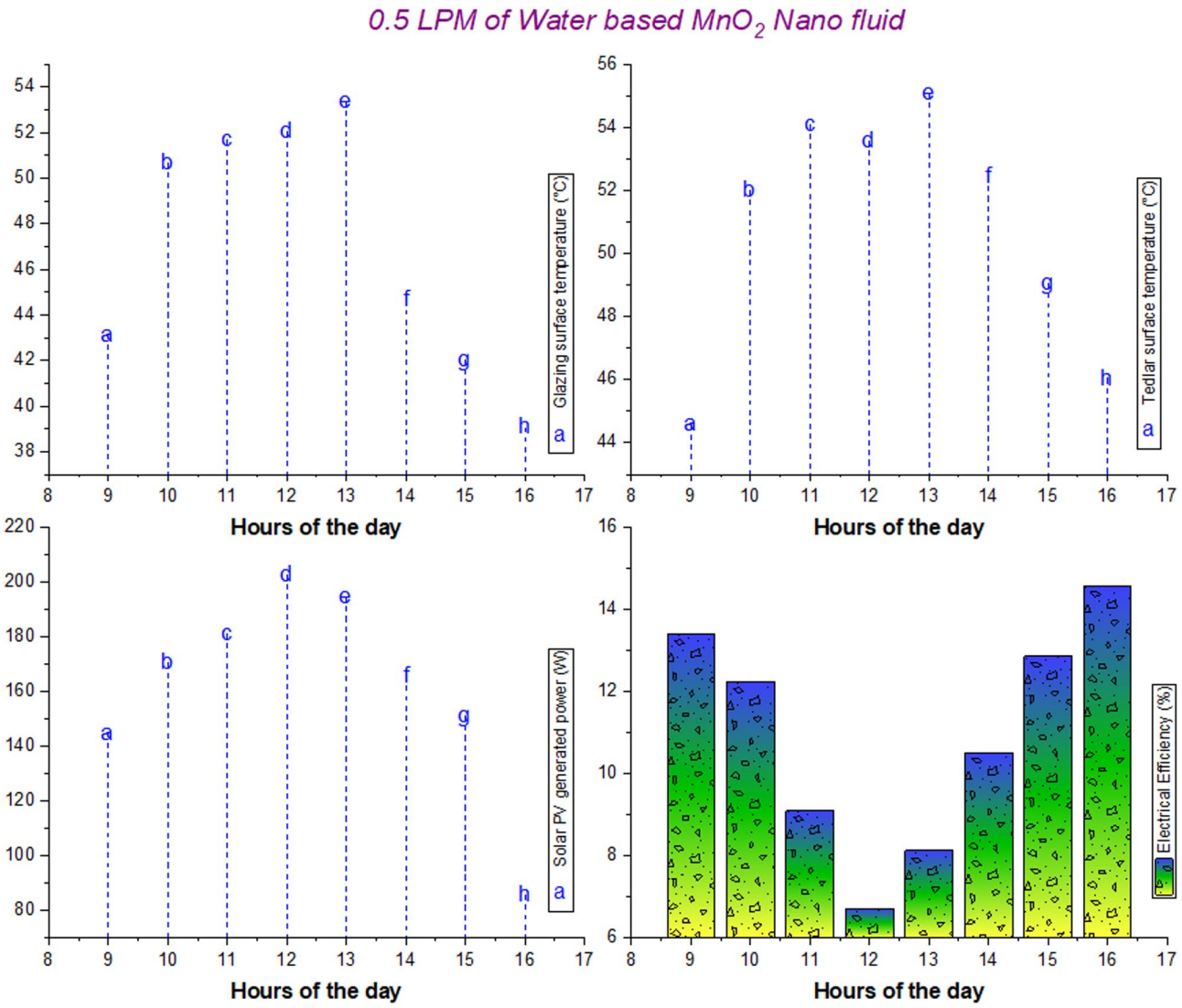

Fig. 15. Various data of 0.5 LPM of water base MnO_2 Nano fluid PVT Collector.

wind speed will come in third. The last one was material properties: higher wind speeds improve convective cooling, which lowers panel temperature and increases efficiency. Heat dissipation is influenced by the glazing and backsheet materials' thermal conductivity and emissivity. Since 0.5 LPM to 0.5 LPM of water base MnO_2 Nano fluid PVT collector was attained its parameters increasing phase namely glazing surface temperature was 52.03 °C by 0.5 LPM of water based MnO_2, 53.31 °C by 1.0 LPM of water based MnO_2, 54.60 °C by 1.5 LPM of water based MnO_2, at noon of the experimental days.

To evaluate the potential for both temperature rise and electrical output, this study first critically examines the role of solar irradiance as the primary driving force in PVT system performance. While increased irradiance typically enhances power generation, it also intensifies thermal loads, necessitating efficient cooling mechanisms to minimize associated efficiency losses. Second, the inverse relationship between ambient temperature and cooling system effectiveness is explored in detail. Elevated ambient temperatures can diminish the cooling system's capacity to remove heat, leading to increased panel temperatures and reduced electrical efficiency. Third, the influence of wind speed on convective cooling is analyzed. Higher wind speeds facilitate enhanced heat dissipation from the glazing surface, thereby lowering the PV panel temperature and improving electrical efficiency. Finally, the thermal properties of system materials—specifically the thermal conductivity and emissivity of the glazing and backsheet—are critically assessed. These material characteristics significantly affect heat dissipation from the PV cells and influence the overall thermal balance of the PVT system, including the efficiency of heat transfer to both the cooling fluid and the external environment.

The glazing surface temperature and its corresponding electrical efficiency were exposed in Fig. 18. When the temperature of the glazing surface increased, the electrical efficiency decreased. These two phenomena were indirectly related to one another. With a glazing surface temperature of 64.23 °C, the equivalent electrical efficiency was 3.12%, whereas with a glazing surface temperature of 48.12 °C, 5.78%. The temperature of the underlying photovoltaic cells directly increases in tandem with an increase in the glazing surface temperature.

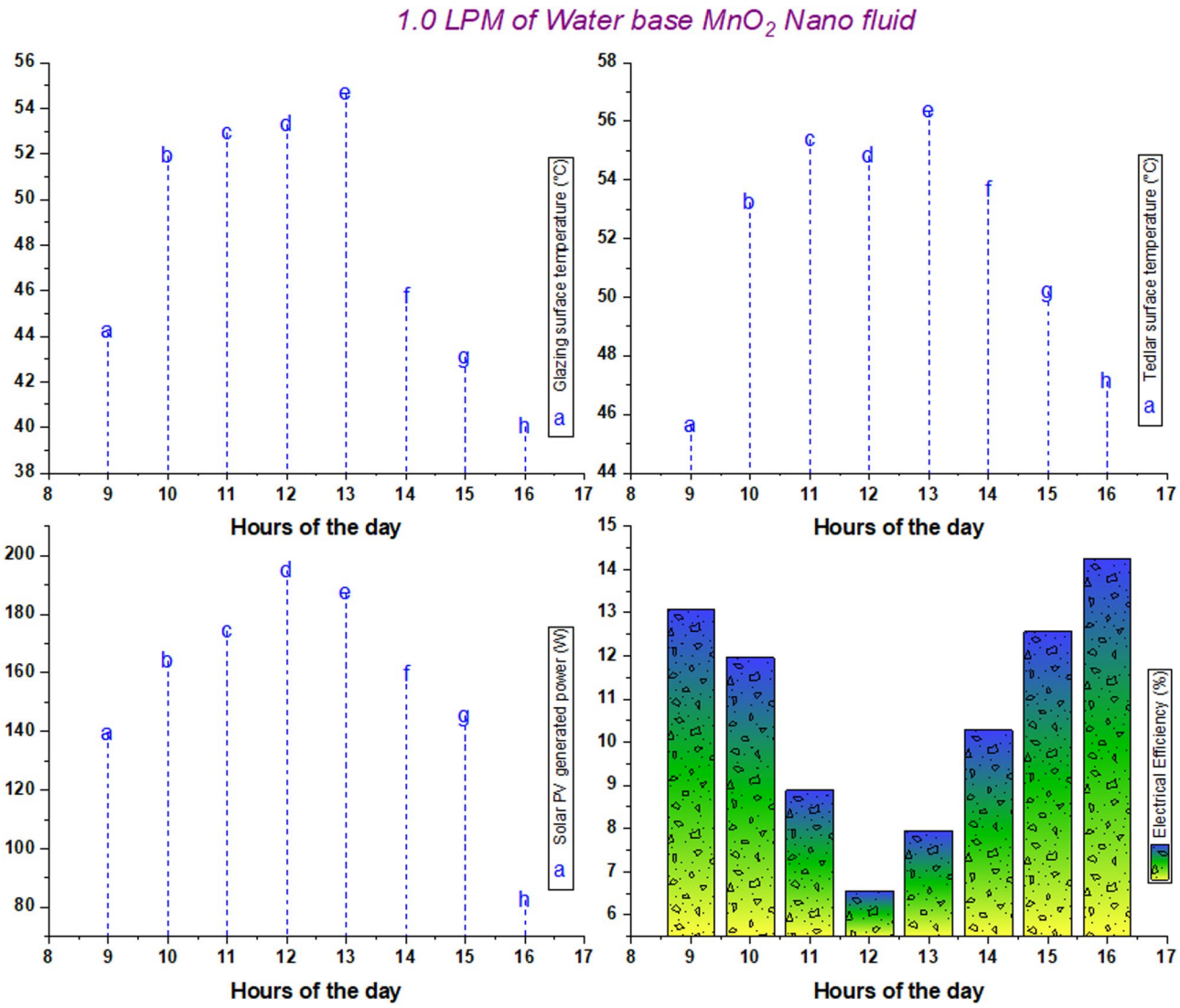

Fig. 16. Various data of 1.0 LPM of water base MnO_2 Nano fluid PVT Collector.

By reducing the bandgap, raising the intrinsic carrier concentration, and quickening the recombination rates in the silicon, this high cell temperature has a significant effect on the characteristics of the semiconductor material. All of these factors work together to lower the PV module's fill factor and open-circuit voltage (Voc), which directly lowers its electrical efficiency. This is well demonstrated by the data in Fig. 17, which shows a significant decrease in electrical efficiency from 5.78% at a glazing temperature of 48.12 °C to a much lower 3.12% at 64.23 °C. This measures the substantial harm that an uncontrolled temperature increase causes to the electrical output.

The glazing surface temperature and its corresponding electrical efficiency were exposed with the three flow rate of water is shown in Fig. 19. In photovoltaic (PV) systems, the glazing surface temperature and electrical efficiency are frequently inversely correlated because of a number of reasons pertaining to the physics of solar cells and how well they function at different temperatures. The effectiveness of solar cells varies with temperature, as indicated by their temperature coefficient. The temperature coefficient for the majority of silicon-based solar cells is negative, which means that the efficiency of the cell falls with rising temperatures. Silicon-based PV modules usually have a temperature coefficient between − 0.3% and − 0.5% per degree Celsius. This indicates a 0.3% to 0.5% drop in the solar cell's electrical efficiency for every degree Celsius as the temperature rises.

The glazing surface temperature and its corresponding electrical efficiency were exposed with the three flow rate of water based MnO_2 is shown in Fig. 20. The electrical characteristics of solar cells, which are composed of semiconductor materials, are temperature-sensitive. The semiconductor material's bandgap shrinks as the solar cell's temperature rises. This lowers the solar cell's overall efficiency by increasing the rate of electron-hole pair recombination. Higher temperatures also cause the semiconductor's inherent carrier concentration to rise, which raises recombination rates and reduces efficiency. As the temperature rises, a solar cell's open-circuit voltage (Voc) falls. This is because more electrons are driven into the conduction band by the heat energy, which lowers the potential difference (voltage) that may be produced. Because voltage and current combine to

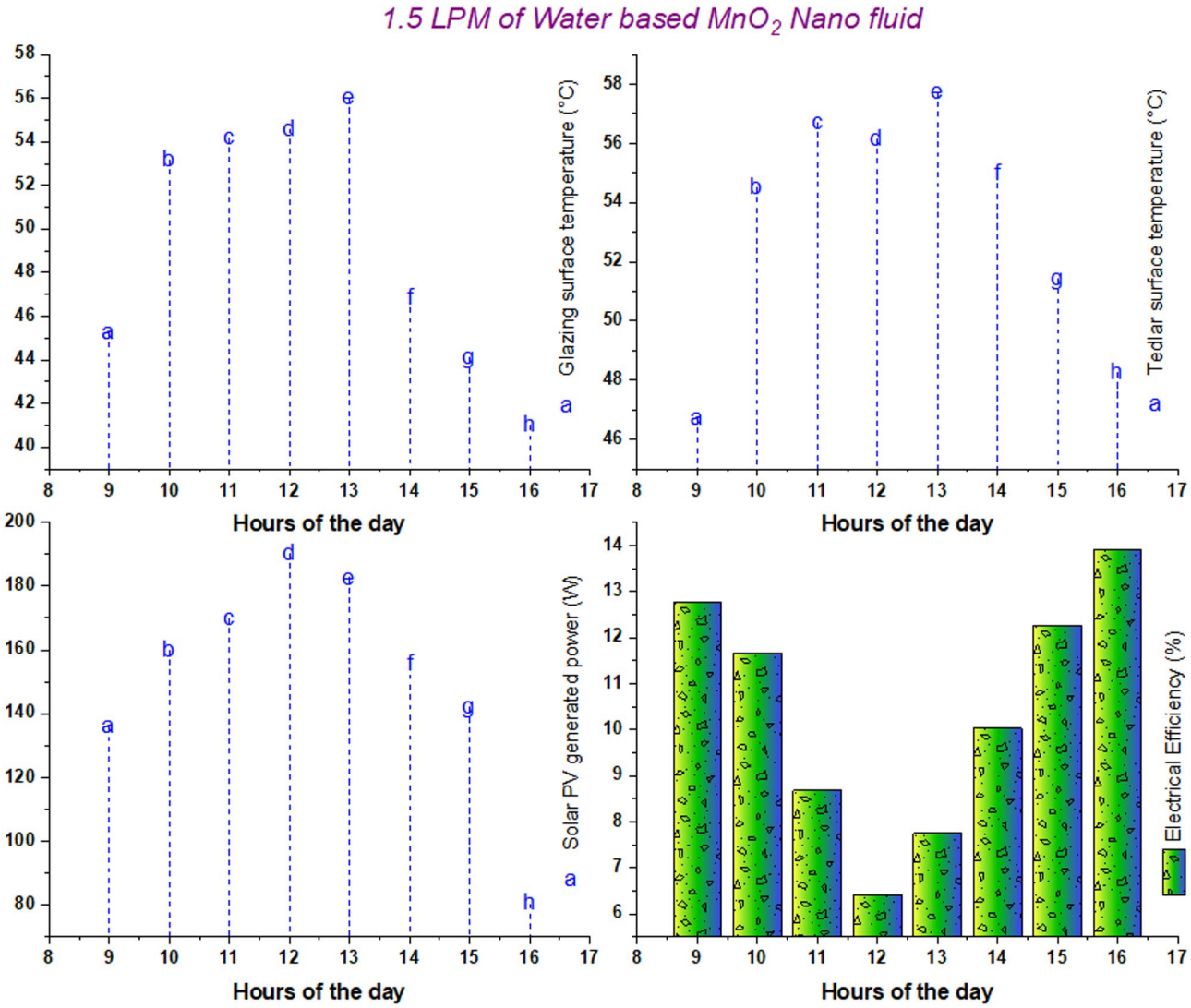

Fig. 17. Diverse data of 1.5 LPM of water base MnO_2 Nano fluid PVT Collector.

determine a solar cell's power output, a drop in voltage always results in a drop in power output and, therefore, efficiency.

The Solar power generation of independent PV, three flow rate of water PVT and three flow rate of water base MnO_2 is shown in Fig. 21. The temperature increase in solar cells can be reduced with the use of efficient thermal management techniques like active or passive cooling. The temperature of the solar cells can, however, increase sharply in many PV systems, particularly those without active cooling, which reduces efficiency. Electrical efficiency is indirectly impacted by the glazing surface temperature, which is a major determinant of the solar panel's total temperature. The lack of cooling features in an independent PV system results in a high surface temperature and limited power output production. Power generation ranges from 64.23 W to 152.36 W. On the other hand, the water-cooled PVT collector had superior power generation results, increasing from 72.48 W to 176.17 W. Ultimately, out of the three power generating modes, the water-based MnO2 nano fluid PVT collector produced superior results. Power supply ranges from 80.42 W to 202.91 W.

The hours of the day variations of PVT module temperature of three water flow rates of present study with PV module temperature of three water flow rates of Praveen kumar and Rajan Kumar 2024 is shown in Fig. 22. While Praveen Kumar and Rajan Kumar 2024[63] conducted experiments in which water was utilised as a cooler for PV modules, this research study shows that the PVT module temperature may be reduced by water. Both PV and PVT module can be cooled by water as coolant because of its life span increasing as well as performance can be increasing. The use of water-based manganese dioxide (MnO_2) nanofluids can substantially enhance the performance of photovoltaic-thermal (PVT) collectors. Compared to conventional standalone PV systems and water-cooled PVT collectors, the MnO_2 nanofluids significantly improve both electrical efficiency and power output. By providing more effective thermal management, the nanofluids help maintain optimal PV panel temperatures, thereby sustaining performance and potentially extending the operational lifespan of the system under real-world conditions. In addition, the integration of machine learning (ML) models—particularly the

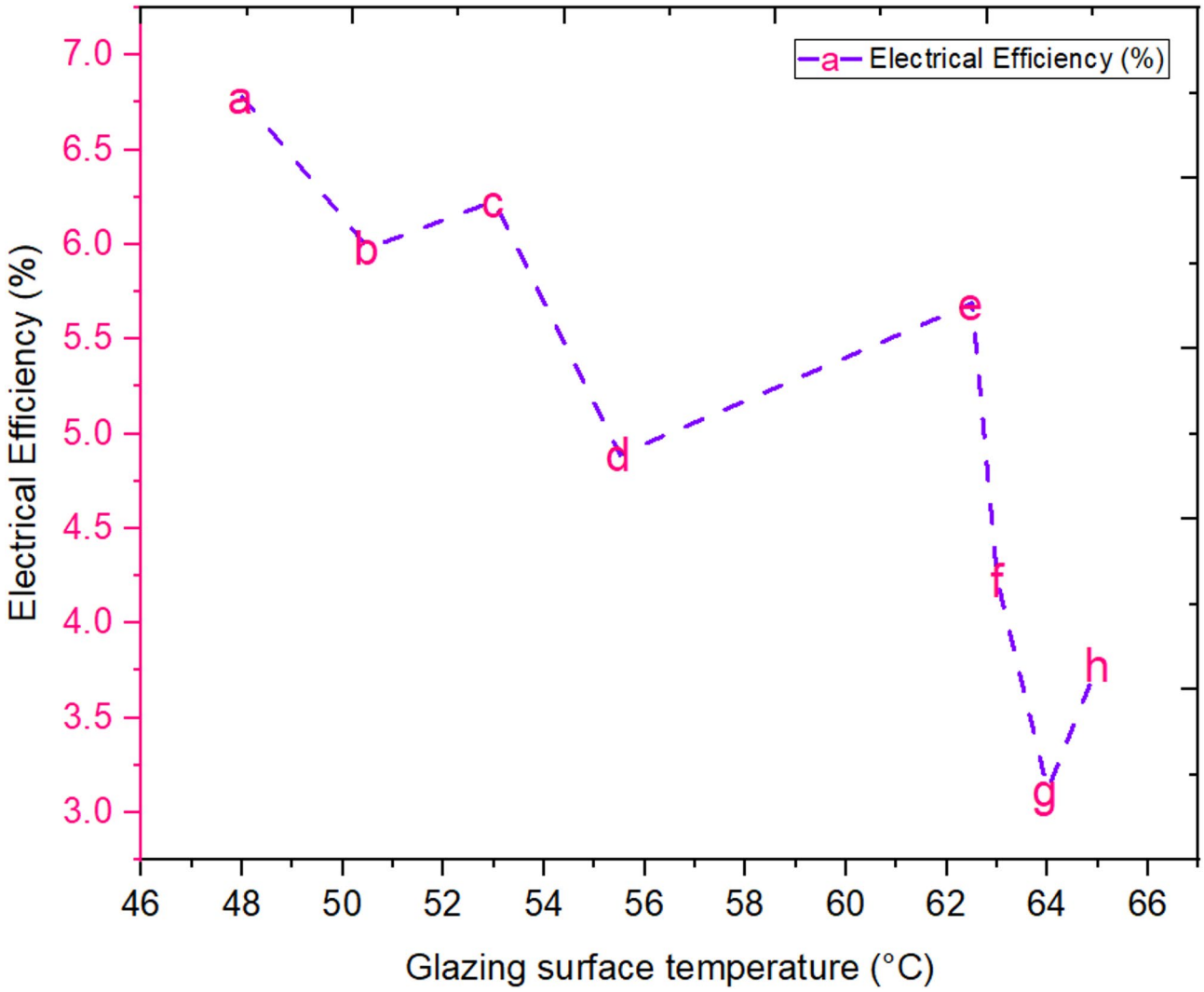

Fig. 18. Glazing surface temperature with electrical efficiency of independent PV.

highly accurate Radial Basis Function (RBF) model—proves to be a powerful tool for predicting and optimizing PVT system behavior. This data-driven approach facilitates intelligent system design and enables real-time performance management. The experimental design incorporated three distinct water flow rates (0.5, 1.0, and 1.5 LPM), which played a crucial role in evaluating the system's robustness and understanding its performance under varying operating conditions. This multi-scenario approach enhances the reliability, applicability, and generalizability of the study's findings.

The hours of the day variations of Thermal exergy, Exergy efficiency, Entropy generation and Exergy destruction of the PVT collector is shown in Fig. 23. The graphs illustrate the performance metrics of a solar system over the course of a day, from 9:00 AM to 4:00 PM. The data shows that Thermal Exergy and Exergy Destruction both follow a similar pattern, peaking around 12:00 PM to 1:00 PM, which corresponds with the period of maximum solar radiation. Specifically, thermal exergy reaches its maximum value of just over 12 W, while exergy destruction peaks at approximately 1600 W. This indicates that while the system is performing at its best in the middle of the day, it is also experiencing the highest rates of energy loss and inefficiency. Conversely, Exergy Efficiency and Entropy Generation show different trends. Exergy efficiency is at its highest in the morning (around 9:00 AM) at just under 19% and again in the late afternoon, dropping to its lowest point of approximately 13.5% around midday. This inverse relationship with solar intensity suggests that the system's efficiency is compromised at peak thermal loads. Meanwhile, Entropy Generation follows a similar trajectory to exergy destruction and thermal exergy, peaking at around 5.2 J/K in the early afternoon, which aligns with the period of highest heat transfer and energy disorder.

Conclusion

The present study demonstrates that the use of water-based manganese dioxide (MnO_2) nanofluids significantly enhances the performance of photovoltaic-thermal (PVT) collectors. By employing three distinct flow rates (0.5, 1.0, and 1.5 LPM), the experimental investigation provided a comprehensive understanding of system behavior

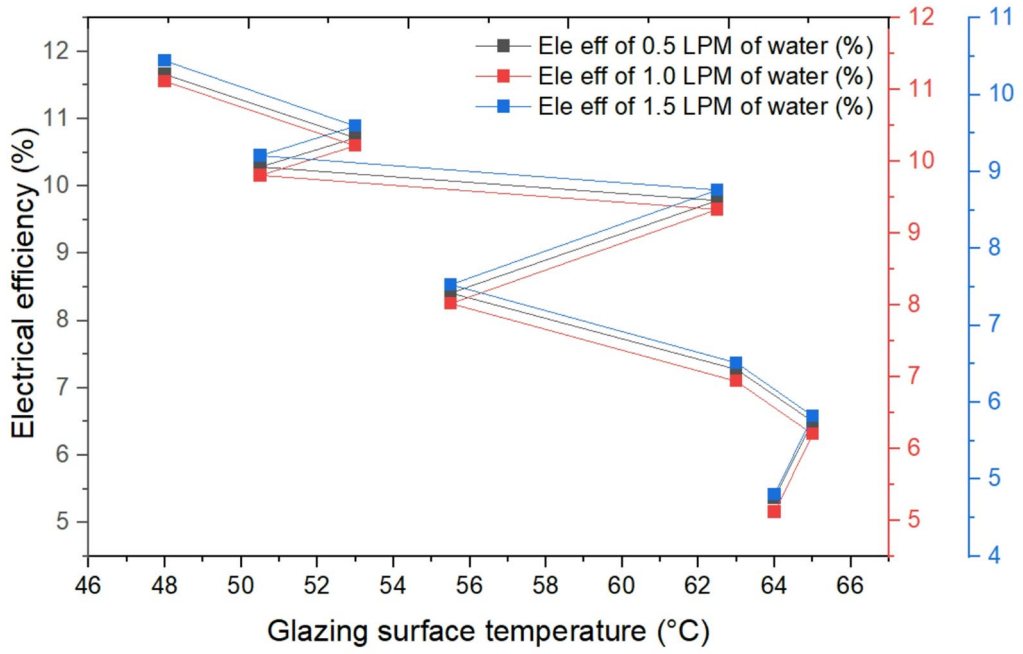

Fig. 19. Glazing surface temperature with electrical efficiency of three flow rate of water.

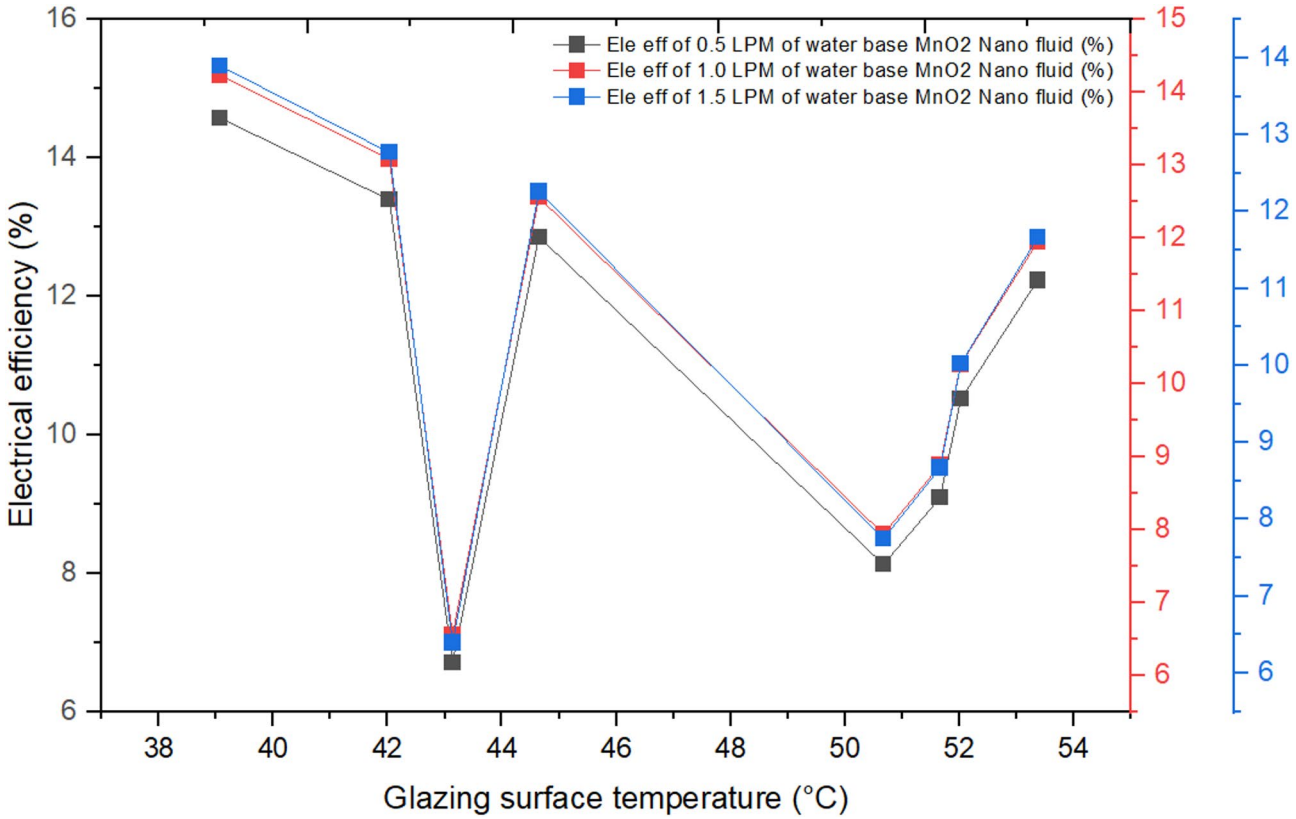

Fig. 20. Glazing surface temperature with electrical efficiency of three flow rate of water with MnO_2 Nanofluid.

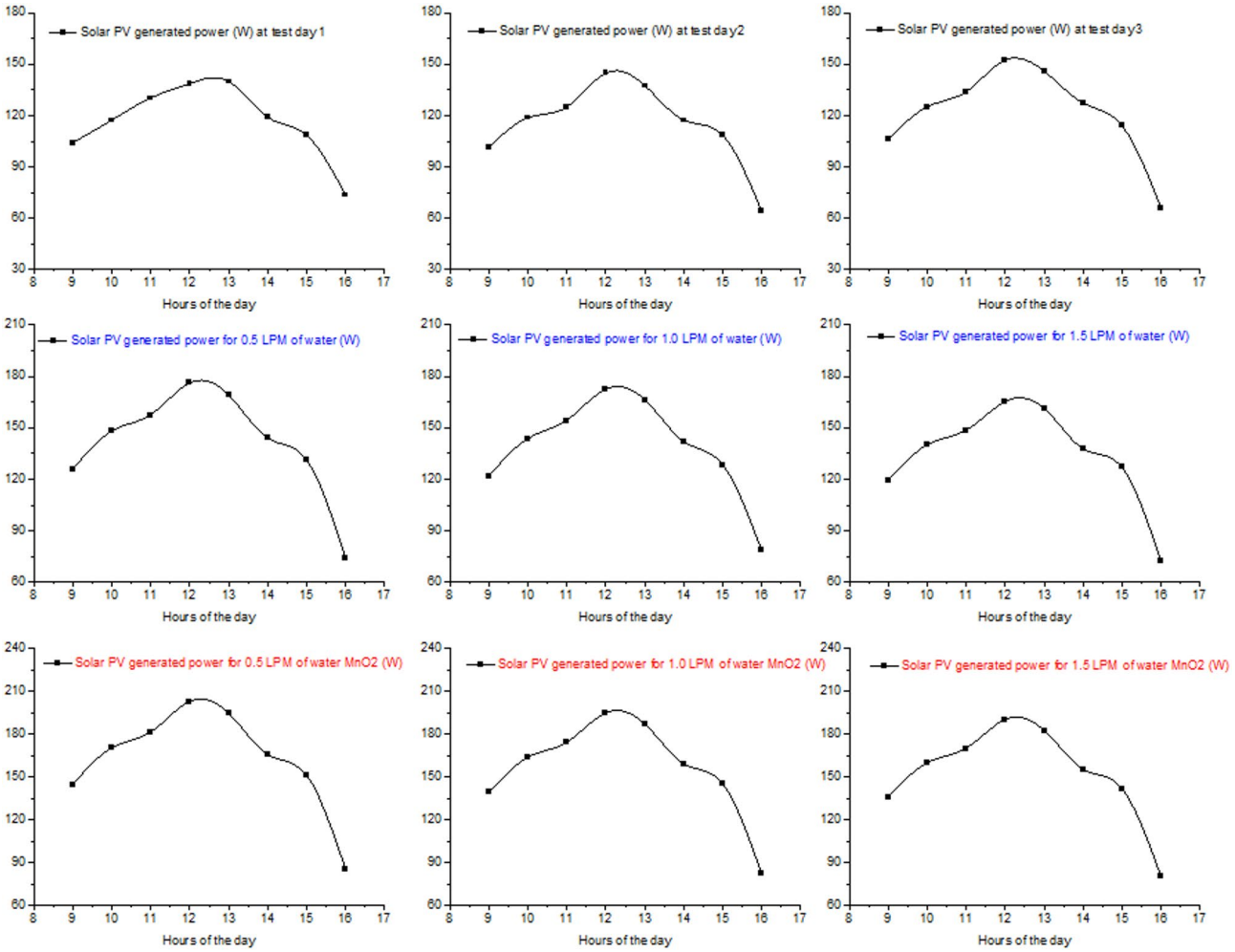

Fig. 21. Solar power generation of independent PV, three flow rate of water PVT and three flow rate of water base Mn Nano fluid.

under varying operational conditions. The MnO_2 nanofluid-based PVT system exhibited superior electrical performance, with power output ranging from 80.42 W to 202.91 W—substantially higher than the standalone PV system, which generated between 64.23 W and 152.36 W. The water-cooled PVT system also outperformed the standalone PV, producing 72.48 W to 176.17 W. Notably, at a flow rate of 0.5 LPM, the MnO_2 nanofluid system achieved a maximum electrical efficiency of approximately 14.58% and a peak power output of 202.91 W; at 1.0 LPM, the efficiency was 14.24%.

The glazing surface temperatures for the MnO_2 nanofluid-based collector were recorded as 52.03 °C (0.5 LPM), 53.31 °C (1.0 LPM), and 54.60 °C (1.5 LPM) at solar noon, indicating effective thermal regulation when compared to the higher surface temperatures of the standalone PV system. In addition to experimental validation, machine learning (ML) models—including Random Forest (RF), Radial Basis Function (RBF), and Multilayer Perceptron (MLP)—were applied to predict system performance. Among them, the RBF model demonstrated superior predictive accuracy, capturing complex non-linear relationships within the thermal and electrical data. It achieved R^2 values of 0.96 for power output and 0.97 for electrical efficiency on the testing dataset. This integrated experimental-ML approach not only confirms the thermal and electrical benefits of MnO_2 nanofluids but also provides a robust framework for optimizing the design and real-time control of high-performance solar energy systems.

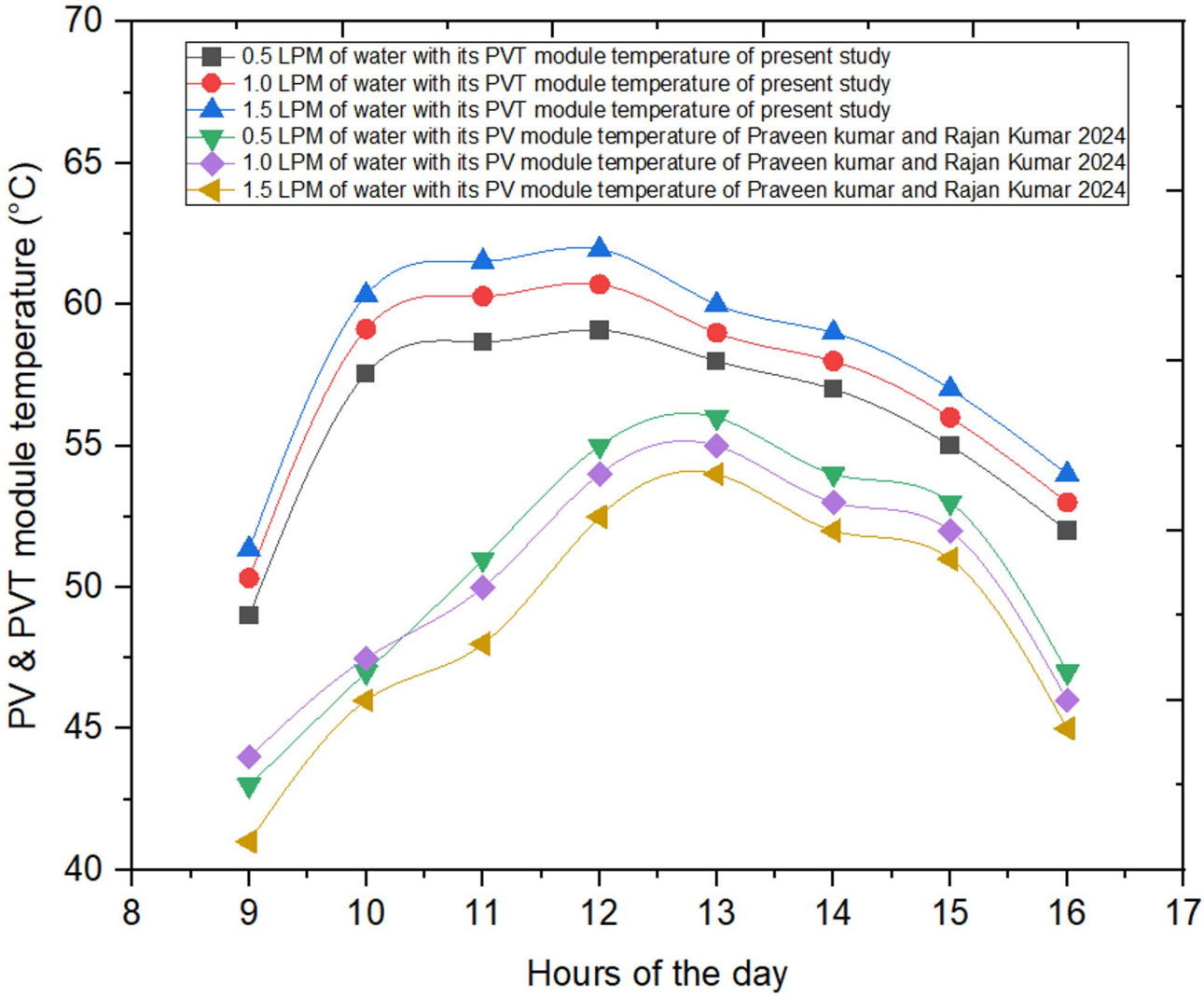

Fig. 22. Variations of PVT module temperature of three water flow rates.

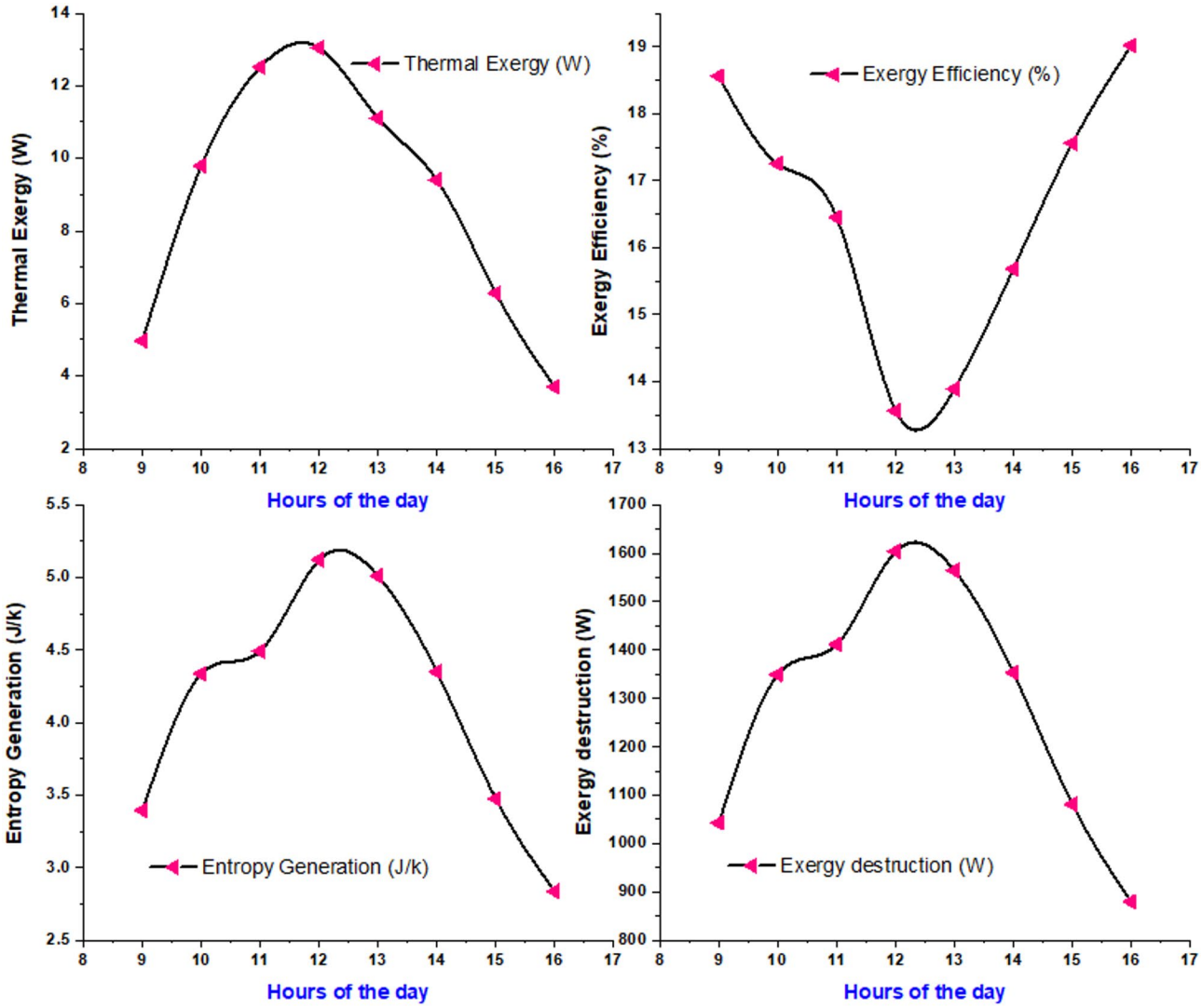

Fig. 23. Thermal exergy, exergy efficiency, entropy generation and exergy destruction of the PVT collector.

Data availability

The datasets used and/or analysed during the current study available from the corresponding author on reasonable request.

Received: 23 April 2025; Accepted: 7 October 2025
Published online: 13 November 2025

References

1. Shi, X. et al. Highly efficient ultra-thin solar selective absorber based on Self-assembled tangent Nano-Ball-Cap arrays. *Chem. Eng. J.* **505**, 159459. https://doi.org/10.1016/j.cej.2025.159459 (2025).
2. Li, Y., Li, H., Miao, R., Qi, H. & Zhang, Y. Energy–Environment–Economy (3E) analysis of the performance of introducing photovoltaic and energy storage systems into residential buildings: A case study in Shenzhen, China. *Sustainability* **15** (11), 9007. https://doi.org/10.3390/su15119007 (2023).
3. Niu, X., Ma, N., Bu, Z., Hong, W. & Li, H. Thermodynamic analysis of supercritical Brayton cycles using CO2-based binary mixtures for solar power tower system application. *Energy* **254**, 124286. https://doi.org/10.1016/j.energy.2022.124286 (2022).
4. Barbosa, E. G. et al. Influence of the absorber tubes configuration on the performance of low cost solar water heating systems. *J. Clean. Prod.* **222**, 22–28 (2019).
5. Al-Waeli, A. H., Chaichan, M. T., Kazem, H. A. & Sopian, K. Comparative study to use nano-(Al2O3, CuO, and SiC) with water to enhance photovoltaic thermal PV/T collectors. *Energy. Conv. Manag.* **148**, 963–973 (2017).
6. Shi, X., Wang, Q. Highly Efficient ultra-thin solar selective absorber based on Self-assembled tangent Nano-Ball-Cap arrays. *Chem Engi J* **505**, 159459. https://doi.org/10.1016/j.cej.2025.159459 (2025).
7. Diwania, S., Agrawal, S., Siddiqui, A. S. & Singh, S. Photovoltaic-thermal (PV/T) technology: a comprehensive review on applications and its advancement. *Int. J. Energy Env Eng.* **11** (1), 33–54 (2020).
8. Pang, G., Xiao, X. & Wang, Y. Preparation and thermal characterization of composite PCMs with modified melting temperature encapsulated in cascade energy storage device for solar heat pump. *J. Energy Storage*. **106**, 114500. https://doi.org/10.1016/j.est.2024.114500 (2025).

9. Sharmila, S. et al. Expediting the bioactivity of zinc sulfide nanoparticles with copper oxide as a nanocomposite. *BMC Chem.* **18**, 204 (2024).
10. Shahsavar, A., Eisapour, M. & Talebizadehsardari, P. Experimental evaluation of novel photovoltaic/thermal systems using serpentine cooling tubes with different cross-sections of circular, triangular and rectangular. *Energy* **208**, 118409 (2020).
11. Zhang, Y., Zhang, Y., Zheng, B., Cui, H. & Qi, H. Statistical analysis for estimating the optimized battery capacity for roof-top PV energy system. *Renew. Energy*. **242**, 122491. https://doi.org/10.1016/j.renene.2025.122491 (2025).
12. Shakir, A. K., Hajidavalloo, E., Daneh-Dezfuli, A., Abdulhaleem, S. M. & Obayes, O. K. Experimental study on the performance of different photovoltaic thermal collectors with nano-technology. *Energy Sources Part. A*. **45**, 8458–8477 (2023).
13. Al-Waeli, A. H. et al. Modeling and experimental validation of a PVT system using nanofluid coolant and nano-PCM. *Sol. Energy*. **177**, 178–191 (2019).
14. Attia, M. E. H. et al. Design and performance optimization of a novel zigzag channeled solar photovoltaic thermal system: numerical investigation and parametric analysis. *J. Clean. Prod.* **434**, 140220 (2024).
15. Niu, X., & Li, H. (2022). Thermodynamic analysis of supercritical Brayton cycles using CO2-based binary mixtures for solar power tower system application. *Energy* **254**, 124286. https://doi.org/10.1016/j.energy.2022.124286.
16. Amalraj, S. & Michael, P. A. Synthesis and characterization of Al2O3 and CuO nanoparticles into nanofluids for solar panel applications. *Results Phys.* **15**, 102797 (2019).
17. Refaey, H. A., Wahba, M. H., Abdelrahman, H. E., Moawad, M. & Berbish, N. S. Experimental study on the performance enhancement of the photovoltaic cells by using various nano-enhanced PCMs. *J. Institution Eng. (India): Ser. C.* **102**, 553–562 (2021).
18. Refaey, H. A. et al. Thermal regulation of photovoltaic panels using PCM with multiple fins configuration: experimental study with analysis. *Therm. Sci. Eng. Progress*. **49**, 102457 (2024).
19. Sharaf, M., Yousef, M. S. & Huzayyin, A. S. Review of cooling techniques used to enhance the efficiency of photovoltaic power systems. *Environ. Sci. Pollut. Res.* **29** (18), 26131–26159 (2022).
20. Shaker, L. M., Al-Amiery, A. A., Hanoon, M. M., Al-Azzawi, W. K. & Kadhum, A. A. H. Examining the influence of thermal effects on solar cells: a comprehensive review. *Sustainable Energy Res.* **11** (1), 6 (2024).
21. Pramanick, D. & Kumar, J. Performance and degradation assessment of two different solar PV cell technologies in the remote region of Eastern India. *e-Prime-Advances Electr. Eng. Electron. Energy*. **7**, 100432 (2024).
22. Shehram, M. Enhancing solar thermal energy storage efficiency to 90% with novel phase change materials PbSO4-NaNO3-NaCl/natural stones. *J. Energy Storage*. **121**, 116481. https://doi.org/10.1016/j.est.2025.116481 (2025).
23. Gharaee, H., Erfanimatin, M. & Bahman, A. M. Machine learning development to predict the electrical efficiency of photovoltaic-thermal (PVT) collector systems. *Energy. Conv. Manag.* **315**, 118808 (2024).
24. Li, Y., Li, H., Miao, R., Qi, H., & Zhang, Y. Energy–Environment–Economy (3E) Analysis of the Performance of Introducing Photovoltaic and Energy Storage Systems into Residential Buildings: A Case Study in Shenzhen, China. *Sustainability* **15**(11), 9007. https://doi.org/10.3390/su15119007 (2023).
25. Varol, Y., Koca, A., Oztop, H. F. & Avci, E. Forecasting of thermal energy storage performance of phase change material in a solar collector using soft computing techniques. *Expert Syst. Appl.* ; **37**(4) (2010).
26. Sheikholeslami, M., Ali, A. & F.A.M Experimental evaluation of vortex generators for enhancing solar photovoltaic panel performance with parabolic reflectors. *Sol. Energy Mater. Sol. Cells*. **282**, 113411 (2025).
27. Sheikholeslami, M. & Alturaihi, M. H. Numerical analysis of thermal management in a photovoltaic solar system with porous heat storage, parabolic reflector and self-cleaning coating. *Int. Commun. Heat Mass Transfer*. **164**, 108847 (2025).
28. Sheikholeslami, M. & Khalili, Z. Simulation of a photovoltaic panel with a novel cooling duct using ternary nanofluid and integrated with a thermoelectric generator. *J. Taiwan Inst. Chem. Eng.* **170**, 105982 (2025).
29. Ali, A. et al. Application of machine learning algorithms in predicting rheological behavior of BN-diamond/thermal oil hybrid nanofluids. *Fluids***9**, 20 (2024).
30. Sankar, A., Gupta, K. K., Bhalla, V. & Pandey, D. S. Multi-criteria optimization of nanofluid-based solar collector for enhanced performance: an explainable machine learning-driven approach. *Energy* **320**, 135212 (2025).
31. Alhamayani, A. & Al-lehaibi, M. The effect of adding hybrid nanoparticles (Al2O3–TiO2) on the performance of parabolic trough solar collectors using different thermal oils and molten salts. *Case Stud. Therm. Eng.* **59**, 104593 (2024).
32. Kanti, P. K. et al. Thermal performance, entropy generation, and machine learning insights of Al_2O_3-TiO_2 hybrid nanofluids in turbulent flow. *Sci. Rep.* **15** (1), 1–20 (2025).
33. Alhamayani, A. Numerical analysis and deep learning algorithm for photovoltaic-thermal systems using various nanofluids and volume fractions at Riyadh, Saudi Arabia. *Case Stud. Therm. Eng.* **54**, 103974 (2024).
34. Alhamayani, A. CNN-LSTM to predict and investigate the performance of a thermal/photovoltaic system cooled by nanofluid (Al2O3) in a hot-climate location. *Processes* **11** (9), 2731 (2023).
35. Margoum, S., Hajji, B., Aneli, S., Tina, G. M. & Gagliano, A. Optimizing nanofluid hybrid solar collectors through artificial intelligence models. *Energies* **17** (10), 2307 (2024).
36. Alhamayani, A. Performance analysis and machine learning algorithms of parabolic trough solar collectors using Al2O3-MWCNT as a hybrid nanofluid. *Case Stud. Therm. Eng.* **57**, 104321 (2024).
37. Sharaby, M. R., Younes, M. M., Abou-Taleb, F. S. & Baz, F. B. The influence of using MWCNT/ZnO-Water hybrid nanofluid on the thermal and electrical performance of a Photovoltaic/Thermal system. *Appl. Therm. Eng.* **248**, 123332 (2024).
38. Sharaby, M. R., Younes, M., Baz, F. & Abou-Taleb, F. State-of-the-Art review: nanofluids for photovoltaic thermal systems. *J. Contemp. Technol. Appl. Eng.* **3** (1), 11–24 (2024).
39. Sharshir, S. W. et al. Degradation mechanisms and stability challenges in perovskite solar cells: a comprehensive review. *Sol. Energy*. **299**, 113707 (2025).
40. Sharaby, M. R., Sharshir, S. W., ElBahloul, A. A., Kandeal, A. W. & Rashad, M. Performance evaluation of fixed and sun-tracking photovoltaic systems integrated with spray cooling. *Sol. Energy*. **288**, 113310 (2025).
41. Kandeal, A. W. et al. Augmentation of the tubular distiller performance via hot air injection from a parabolic trough collector, nanocoating, and nanofluid. *Sol. Energy*. **277**, 112743 (2024).
42. Sharshir, S. W. et al. Utilizing a novel metal-organic framework for clean water production: synergistic evaporation boost in double slope distiller. *Case Stud. Therm. Eng.* **68**, 105876 (2025).
43. Gupta, M. K., Kumar, Y., Sonnathi, N. & Sharma, S. K. Synthesis of MnO2 nanostructure and its electrochemical studies with ratio optimization of ZnO. *Ionics* **29**(7), 2959–2968 (2023).
44. Agrawal, S. & Tiwari, A. Experimental validation of glazed hybrid micro-channel solar cell thermal tile. *Sol Energy*. **85** (5), 3046–3056 (2011).
45. Wei, T., Zhang, Y., Zhang, Y., Miao, R., Kang, J.,... Qi, H. City-scale roof-top photovoltaic deployment planning. *Appl Energy* **368**, 123461. https://doi.org/10.1016/j.apenergy.2024.123461 (2024).
46. Amini, S., Taki, M. & Rohani, A. Applied improved RBF neural network model for predicting the broiler output energies. *Appl. Soft Comput. J.* **87**, 106006 (2020).
47. Ko, C. N. & Lee, C. M. Short-term load forecasting using SVR (support vector regression)- based radial basis function neural network with dual extended Kalman filter. *Energy* **49**, 413–422 (2013).
48. Haykin, S. S. *Neural Networks and Learning Machines* (Pearson, 2009).

49. Rohani, A., Taki, M. & Abdollahpour, Z. A novel soft computing model (Gaussian process regression with K-fold cross validation) for daily and monthly solar radiation forecasting (Part: I). *Renew. Energy*. **115**, 411–422 (2018).
50. Taki, M., Rohani, A., Yildizhan, H. & Farhadi, R. Energy-exergy modeling of solar radiation with most influencing input parameters, energy Sources, part A Recovery, util. *Environ. Eff.* **41** (17), 2128–2144 (2019).
51. Elangovan, M., Srimanickam, B., Čep, R., Saranya, A. & Ramachandran, M. Experimental study of a hybrid solar collector using TiO2/water nanofluids. *Energies* **15** (12), 4425 (2022).
52. Christopher Selvam, D. et al. Advances in nano-enhanced phase change materials and hybrid thermal energy storage systems: paving the way for sustainable energy solutions. *Results Eng.* **27**, 105729. https://doi.org/10.1016/j.rineng.2025.105729 (2025).
53. Jayaprakash, G. S., Beemkumar, N., Sunil Kumar, M., Kamakshi Priya, K. & Kaliappan, N. Experimental investigation of cascaded thermal energy storage systems using finned encapsulated phase change materials. *Results Eng.* **25**, 104395. https://doi.org/10.1016/j.rineng.2025.104395 (2025).
54. Akbar, A., Abas, N., Saleem, M. S., Rauf, S. & Haider, A. Enhancing solar energy efficiency with hybrid CSP systems: design and analysis of a parabolic dish collector integrated with thermal energy storage. *Clean. Eng. Technol.* **27**, 101043. https://doi.org/10.1016/j.clet.2025.101043 (2025).
55. Hekimoglu, G. Development of sustainable composite PCMs using bio-derived activated carbon hybrid matrices for enhanced thermal energy storage efficiency. *Diam. Relat. Mater.* **154**, 112224. https://doi.org/10.1016/j.diamond.2025.112224 (2025).
56. Zhang, Y., Zhang, Y., Zheng, B., Cui, H., & Qi, H. Statistical analysis for estimating the optimized battery capacity for roof-top PV energy system. *Renewable Energy* **242**, 122491. https://doi.org/10.1016/j.renene.2025.122491 (2025).
57. Tiwari, G. N. & Al-Helal, I. M. Analytical expression of temperature dependent electrical efficiency of N-PVT water collectors connected in series. *Sol. Energy*. **114**, 61–76 (2015).
58. Guruprasad, B., Srimanickam, B., Natarajan, U., Malayalamurthi, R. & Elango, A. Performance investigation on various models on solar photovoltaic thermal (PVT) hybrid system. In *AIP Conference Proceedings* Vol. 2161 (AIP Publishing, 2019).
59. Jayaprakash, G. S., Beemkumar, N., Sunil Kumar, M. & Kamakshi Priya, K. Nandagopal Kaliappan Enhancing Thermal Energy Storage Efficiency: Synthesis and Analysis of Hybrid Nano-PCMs. *Results Eng.* **26**: 104899. https://doi.org/10.1016/j.rineng.2025.104899. (2025).
60. Al-Shamani, A. N. et al. Experimental studies of rectangular tube absorber photovoltaic thermal collector with various types of nanofluids under the tropical climate conditions. *Energy. Conv. Manag.* **124**, 528–542 (2016).
61. Jia, Y., Alva, G. & Fang, G. Development and applications of photovoltaic–thermal systems: A review. *Renew. Sustain. Energy Rev.* **102**, 249–265 (2019).
62. Hasan, A., McCormack, S. J., Huang, M. J. & Norton, B. Energy and cost saving of a photovoltaic-phase change materials (PV-PCM) system through temperature regulation and performance enhancement of photovoltaics. *Energies* **7** (3), 1318–1331 (2014).
63. Tyagi, P. K. & Kumar, R. Comprehensive performance assessment of photovoltaic/thermal system using MWCNT/water nanofluid and novel finned multi-block nano-enhanced phase change material-based thermal collector: Energy, exergy, economic, and environmental (4E) perspectives. *Energy* **312**, 133575 (2024).

Author contributions
All authors have equally contributed to the manuscript.

Declarations

Competing interests
The authors declare no competing interests.

Additional information
Correspondence and requests for materials should be addressed to N.K.

Reprints and permissions information is available at www.nature.com/reprints.

Publisher's note Springer Nature remains neutral with regard to jurisdictional claims in published maps and institutional affiliations.